Automated Photoluminescence Experimentation for Understanding Dynamic Metal-Halide Perovskite Semiconductors

Kiligaridis, Alexander

2023

Document Version:
Publisher's PDF, also known as Version of record

Automated Photoluminescence Experimentation for Understanding Dynamic Metal-Halide Perovskite Semiconductors

ALEXANDER KILIGARIDIS
DEPARTMENT OF CHEMISTRY | FACULTY OF SCIENCE | LUND UNIVERSITY

Automated Photoluminescence Experimentation for Understanding Dynamic Metal-Halide Perovskite Semiconductors

Alexander Kiligaridis

LUND
UNIVERSITY

DOCTORAL DISSERTATION

by due permission of the Faculty of Science, Lund University, Sweden. To be defended at Lecture hall B, Kemicentrum, Naturvetarvägen 16, 22362 Lund, Monday the 20th of November 2023 at 9:00 am.

Faculty opponent
Prof. Dr. Thomas Kirchartz

Organization: LUND UNIVERSITY, Division of Chemical Physics Department of Chemistry Box 124 SE-221 00 Lund, Sweden

Document name: Doctoral Dissertation **Date of issue**:

Author(s): Alexander Kiligaridis **Sponsoring organization:**

Title and subtitle: Automated Photoluminescence Experimentation for Understanding Dynamic Metal-Halide Perovskite Semiconductor

Abstract: Metal halide perovskites have garnered significant attention for their remarkable optoelectronic properties and unique photophysical characteristics. Combined with low cost for fabrication, this new class of materials is among the most promising candidates within next generation photovoltaic technologies. However, the complex nature of metal halide perovskites' crystal structures and compositions requires precise control during synthesis to achieve desired properties. Small variations in composition can significantly impact the material's behavior, demanding meticulous experimentation and characterization. Another challenge associated with the research of perovskite metal halides is the observer effect, a concept most often associated with quantum mechanics and refers to the alteration of a state by the act of observing it. In the context of perovskite materials, the very act of measurement or characterization can influence the material's behavior, potentially leading to discrepancies between observed and actual properties. Photoluminescence spectroscopy is a powerful analytical technique that plays a pivotal role in unraveling the optical properties and electronic behavior of perovskite materials. The emission of light upon excitation provides insights into the material's band structure, defect states and recombination dynamics. This thesis presents a comprehensive exploration of the convergence between photoluminescence spectroscopy and automation testing techniques, tailored to the specific requirements of metal halide perovskite materials. The integration of these two domains offers a novel approach to accelerate the characterization of the optoelectronic properties of metal halide perovskites. The integration of automation not only enhances the efficiency of experimentation but also enables the exploration of a wider parameter space. One of the examples that we will present in this work is a novel experimental methodology, incorporating photoluminescence measurements within a two-dimensional parameter space of excitation energy and laser pulse repetition frequency. We demonstrate the effectiveness of this technique in comprehensively investigating the dynamic photochemical properties of our material due to sample aging and degradation, photo-induced reversible and irreversible processes during the act of measuring.

Key words: Photoluminescence, Perovskites, Semiconductor, Spectroscopy, Microscopy

Classification system and/or index terms (if any)

Supplementary bibliographical information

Language: English **ISSN and key title**:

ISBN: 978-91-7422-998-1

Recipient's notes **Number of pages**: 56

Price Security classification

Signature Date 2023-10-12

Automated Photoluminescence Experimentation for Understanding Dynamic Metal-Halide Perovskite Semiconductors

Alexander Kiligaridis

LUND
UNIVERSITY

Coverpicture by Yana Vaynzof

Faculty of Science, Department of Chemistry - Division Chemical Physics

isbn: 978-91-7422-998-1 (print)

isbn: 978-91-7422-999-8 (pdf)

Printed in Sweden by Media-Tryck, Lund University

Lund 2023

Αφιερωμένο στους γονείς μου,
Ανδρονίκη και Γρηγόρη
και στην αδερφή μου Κατερίνα

Table of Contents

Abstract

Metal halide perovskites have garnered significant attention for their remarkable optoelectronic properties and unique photophysical characteristics. Combined with low fabrication cost, this new class of materials is among the most promising candidates within the next generation photovoltaic technologies.

However, the complex nature of metal halide perovskites' crystal structures and compositions requires precise control during synthesis to achieve desired properties. Small variations in composition can significantly impact the material's behavior, demanding meticulous experimentation and characterization. Another challenge associated with the research of metal halide perovskites is the observer effect, a concept most often associated with quantum mechanics and refers to the alteration of a quantum system state by the act of observing it. In the context of perovskite halides materials, the very act of measurement or characterization can influence the material's behavior, potentially leading to discrepancies between observed and actual properties.

Photoluminescence spectroscopy is a powerful analytical technique that plays a pivotal role in unraveling the optical properties and electronic behavior of perovskite materials. The emission of light upon excitation provides insights into the material's band structure, defect states and charge recombination dynamics.

This thesis presents a comprehensive exploration of the convergence between photoluminescence spectroscopy and automation testing techniques, tailored to the specific requirements of the metal halide perovskite materials. The integration of these two domains offers a novel approach to accelerate the characterization of the optoelectronic properties of metal halide perovskites. The integration of automation not only enhances the efficiency of experimentation but also enables the exploration of a wider parameter space which is otherwise out of practical reach.

One of the examples that is presented in this work is a novel experimental methodology, incorporating photoluminescence measurements within a two-dimensional parameter space of the excitation energy and the laser pulse repetition frequency. We demonstrate the effectiveness of this technique by employing it to investigate the dynamic photochemical properties of our materials due to sample aging and degradation, as well as photo-induced reversible and irreversible processes during the act of measuring.

Popular Science Summary

Perovskite metal halides are a fascinating group of materials with incredible potential for revolutionizing technology, particularly in fields like solar energy and lighting. These materials exhibit remarkable optoelectronic properties that make them highly sought after for various applications. However, delving into the secrets of these materials comes with its own set of challenges, one of which is known as the observer effect.

Imagine trying to study something so delicate that just looking at it can change its behaviour. That is the predicament researchers face when investigating perovskite metal halides. The observer effect refers to how the act of observing or measuring these materials can alter their properties. It is like trying to take a photo of a butterfly without scaring it away – the mere presence of the observer can cause changes that you are trying to capture.

Perovskite metal halides are sensitive to light, heat, and even the equipment used for measurements. This means that when researchers try to understand their properties, they unintentionally modify them. It is as if the act of looking causes the material to change its behaviour, making it challenging to get accurate data about its true nature.

Despite the challenges, researchers are making significant strides in overcoming the observer effect. By collaborating across disciplines and using advanced technology, they are working to uncover the true potential of perovskite metal halides. The goal is to find ways to study these materials without altering their behaviour and to harness their incredible properties for efficient solar cells, better lighting, and more.

So, next time you hear about perovskite metal halides and their potential to change the way we power our world, remember the hidden challenge of the observer effect that researchers are tackling to unveil their secrets.

Populärvetenskaplig Sammanfattning

Perovskitmetallhalider är en fascinerande grupp material med otrolig potential att revolutionera teknologin, särskilt inom områden som solenergi och belysning. Dessa material uppvisar enastående optoelektroniska egenskaper som gör dem mycket eftertraktade för olika tillämpningar. Men att utforska dessa materials hemligheter kommer med sina egna utmaningar, varav en är känd som observatörseffekten.

Föreställ dig att försöka studera något så känsligt att bara att titta på det kan ändra dess beteende. Det är den situation forskare står inför när de undersöker perovskitmetallhalider. Observatörseffekten hänvisar till hur själva handlingen att observera eller mäta dessa material kan ändra deras egenskaper. Det är som att försöka ta en bild av en fjäril utan att skrämma den bort - observatörens närvaro kan orsaka förändringar som du försöker fånga.

Perovskitmetallhalider är känsliga för ljus, värme och till och med utrustningen som används för mätningar. Det innebär att när forskare försöker förstå deras egenskaper, ändrar de oavsiktligt på dem. Det är som om själva handlingen att titta på materialet får det att ändra beteende, vilket gör det svårt att få noggranna data om dess sanna natur.

Trots utmaningarna gör forskare betydande framsteg när det gäller att övervinna observatörseffekten. Genom samarbete över discipliner och användning av avancerad teknik arbetar de för att avslöja perovskitmetallhaliders sanna potential. Målet är att hitta sätt att studera dessa material utan att ändra deras beteende och dra nytta av deras otroliga egenskaper för effektiva solceller, bättre belysning och mer.

Så nästa gång du hör talas om perovskitmetallhalider och deras potential att förändra sättet vi driver vår värld på, kom ihåg den dolda utmaningen med observatörseffekten som forskare kämpar med för att avslöja deras hemligheter.

Acknowledgments

Firstly, I want to say a big thank you to my supervisor, Ivan. You have been a tremendous support throughout my PhD journey and research. We have had many interesting discussions about both work and personal matters, and I truly appreciate your mentorship and encouragement.

I am also grateful to my mentor and friend, Aboma, for introducing me to the world of research and for being a significant influence on my career. Your dedication and inspiration have played a crucial role in my academic and professional development.

Being part of the Single Molecule Spectroscopy group has been a wonderful experience. We have worked together, enjoyed pizza nights, and had fun outings to Ivan's country house. I am thankful for the friendship and the great memories we've made together.

I would also like to thank all the members of the Chemical Physics division for creating a positive work environment and organizing fun social activities. Your collective efforts have made my academic journey rewarding and enjoyable.

List of Papers

Paper I

Excitation wavelength dependence of photoluminescence flickering in degraded $MAPbI_3$ perovskite and its connection to lead iodide formation.

Alexander Kiligaridis, Aboma Merdasa, Carolin Rehermann, Eva L. Unger, Ivan G. Scheblykin. *Journal of Luminescence*, Volume 222, 117129, (2020). doi:10.1016/j.jlumin.2020.117129

Assisted AM in designing and calibrating the experimental setup. Analysed the data and wrote the manuscript together with IGS.

Paper II

Impact of Excess Lead Iodide on the Recombination Kinetics in Metal Halide Perovskites

Aboma Merdasa, **Alexander Kiligaridis**, Carolin Rehermann, Mojtaba Abdi-Jalebi, Jonas Stöber, Boris Louis, Marina Gerhard, Samuel D. Stranks, Eva L. Unger, Ivan G. Scheblykin. *ACS Energy Letters*, s. 1370-1378, (2019). doi:10.1021/acsenergylett.9b00774

Assisted AM in designing and calibrating the experimental setup. Also assisted AM in the experimental measurements.

Paper III

Are Shockley-Read-Hall and ABC models valid for lead halide perovskites?

Alexander Kiligaridis, Pavel A. Frantsuzov, Aymen Yangui, Sudipta Seth, Jun li, Qingzhi An, Yana Vaynzof, Ivan G. Scheblykin. *Nature Communications* 12, 3329, (2021). doi:10.1038/s41467-021-23275-w

Built the optical setup together with IGS. Designed the automated experimental protocol and its practical realization. Wrote the software to control the experimental setup and performed the measurements together with AY. Wrote the analysis software and performed the analysis on the experimental data. Wrote the manuscript together with IGS.

Paper IV

Photoluminescence Mapping over Laser Pulse Fluence and Repetition Rate as a Fingerprint of Charge and Defect Dynamics in Perovskites.

Shraddha M. Rao, **Alexander Kiligaridis**, Aymen Yangui, Qingzi An, Yana Vaynzof, Ivan G. Scheblykin. *Advanced Optical Materials*, 2300996, (2023). doi:10.1002/adom.202300996

Built the optical setup together with IGS. Wrote the software to control the experimental setup. Wrote the analysis software.

Abbreviations

CW – Continuous-Wave

EM-CCD – Electron Multiplying Charge-Coupled Device

MAPI – Methylammonium Lead Iodide

MHP – Metal Halide Perovskite

OD – Optical Density

PL – Photoluminescence

PLE – Photoluminescence Excitation

PLQY – Photoluminescence Quantum Yield

PSC – Perovskite Solar Cell

SRH – Shockley-Read-Hall

TRPL – Time Resolved Photoluminescence

Chapter 1 Introduction

1.1 Metal Halide Perovskite Materials

In the past decade, metal halide perovskites (MHPs) have become a promising star in the field of optoelectronics. The optoelectronic technologies based on MHPs, such as perovskite solar cells (PSCs), light emitting diodes, photodetectors and lasers, have been advancing the current paradigm due to the remarkable optoelectronic properties of MHPs.[1–4] This family of compounds, having the general formula of ABX_3 ($A = CH_3NH_3^+$ (MA), $HC(NH_2)_2^+$ (FA), and Cs^+, $B = Pb^{2+}$, Sn^{2+}, $X = I^-$, Cl^-, Br^-), has the advantages of easy and cost-efficient preparation. The crystal structure and chemical composition of MHPs give them their unique characteristics, including high optical absorption, high carrier mobility and long diffusion lengths,[5–9] while also enabling a high degree of flexibility and tunability.[10–12]

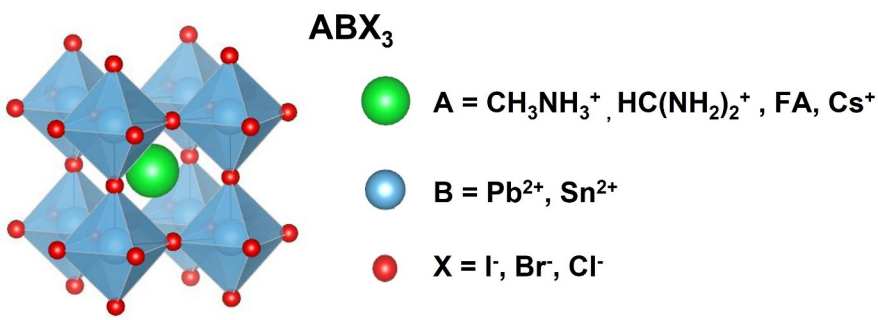

Figure 1. Structure of a metal halide perovskite with the general chemical formula ABX_3.

The typical ABX_3 perovskite has B at the centre of an octahedral $[BX_6]^{4-}$ cluster, with the BX_6 framework made up of corner-shared octahedrons. A is arranged in a 12-fold cuboctahedral coordination with X anions, located between the octahedral BX_6 framework (Figure 1).

The power conversion efficiency of PSCs has been improved from an initial 3.8% in 2009[13], to 25.7%, 28% and 31.3%, for single-junction PSCs, all-perovskite tandem solar cells and hybrid tandem PSCs respectively[14].

Despite of their remarkable properties and promising efficiencies in devices, there are great challenges in the research of MHP's, originating in both their long-term instability and also temporary and reversible photo-induced changes in the material when illuminated. In this thesis, I will present new experimental methods to further elucidate the optoelectronic properties of MHP's, specifically designed to take into account any changes introduced to the material by the act of studying it through light illumination.

1.2 Photophysics of Semiconductors

1.2.1 Charge Carrier Recombination in Direct Bandgap Semiconductors

Free charge carriers can be generated in a semiconductor when light with sufficient energy is absorbed, exciting electrons from the valence band, across the band gap to the conduction band. After the generation of a free electron-hole pair has occurred, the semiconductor system can return to its ground state when the mobile charge carriers have been eliminated through a variety of possible relaxation routes.

In the case of direct bandgap semiconductors, the three primary pathways for recombination are: radiative (band to band) recombination, trap-assisted non-radiative, and Auger recombination. The total energy of the system must be conserved.

(i) During the radiative band-to-band recombination, an electron-hole pair is annihilated, and the energy is emitted as a photon to produce photoluminescence (PL) emission.

(ii) In the case of trap-assisted non-radiative recombination, the excited carriers are trapped by crystal defect sites, and the energy is released as phonons progressively relaxing towards the ground state.

(iii) Finally, in the process of Auger recombination, which is also non-radiative, the excess energy released from the electron-hole recombination is transferred to a third charge carrier, which is excited to a higher energy level.

1.2.2 Shockley-Read-Hall and ABC Recombination Models

One of the models describing the kinetics of charge carrier concentrations in a semiconductor with defect states was proposed by Shockley and Read[15] and

independently by Hall[16] and is known as the Shockley–Read–Hall (SRH) model. It is important to note that in the SRH model the concentration of free electron can be different from the concentration of free holes, due to trapping in the defect states. Furthermore, only the non-radiative recombination of trapped electrons and free holes as well as the radiative band-to-band recombination are considered (the first and second order kinetic processes respectively). One possible realization of the model can be described by the following set of equations:

$$\frac{d}{dt}n(t) = G(t) - k_r np - k_t(N - n_t)n \qquad (1)$$

$$\frac{d}{dt}n_t(t) = k_t(N - n_t) - k_n n_t p \qquad (2)$$

$$\frac{d}{dt}p(t) = G(t) - k_r np - k_n n_t p \qquad (3)$$

Where $G(t)$ is density of the photogenerated carriers per second [$\mathrm{cm}^{-3}s^{-1}$], $n(t)$,$n_t(t)$ and $p(t)$ are the densities of electrons in the conduction band, trapped electrons and holes respectively (charge conservation: $n(t) + n_t(t) = p(t)$), N is the density of traps. k_r,k_t and $k_n$are radiative electron-hole recombination rate, electron trapping rate and non-radiative recombination rate of a trapped electron and a free hole respectively, see the scheme in Figure 2.

Shen et al.[17] suggested another simplified model called ABC, to account for the missing third order processes, most importantly the non-radiative Auger recombination. The name derives from the coefficients A, B, and C for the first-order (monomolecular), second-order (bi-molecular), and third-order Auger recombination, respectively, and the model is described by the equation

$$\frac{d}{dt}n(t) = -An - Bn^2 - Cn^3 \qquad (4)$$

An important difference between the two models is that in the ABC the concentration of free electrons and holes are always equal, which is not necessarily the case for the SRH due to presence of long-lived trapped charge carriers.

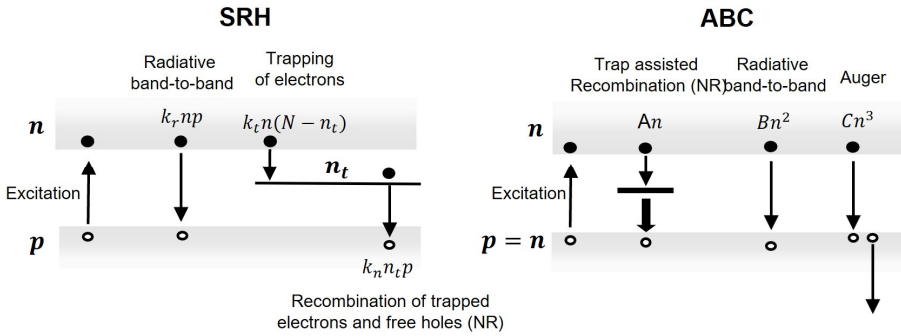

Figure 2. The energy level scheme and charge recombination processes of the SRH and ABC models.

1.2.3 Photoluminescence Emission

As mentioned earlier, during band-to-band recombination of free charge carriers in a direct band gap material, the energy is released in the form of emitting photons, the photoluminescence phenomenon. The physical processes involved in photoluminescence are much more intricate than absorption due to its close connection with the energy relaxation mechanisms within the solid. The emission spectrum is further influenced by the thermal distribution of electrons and holes in their respective bands.

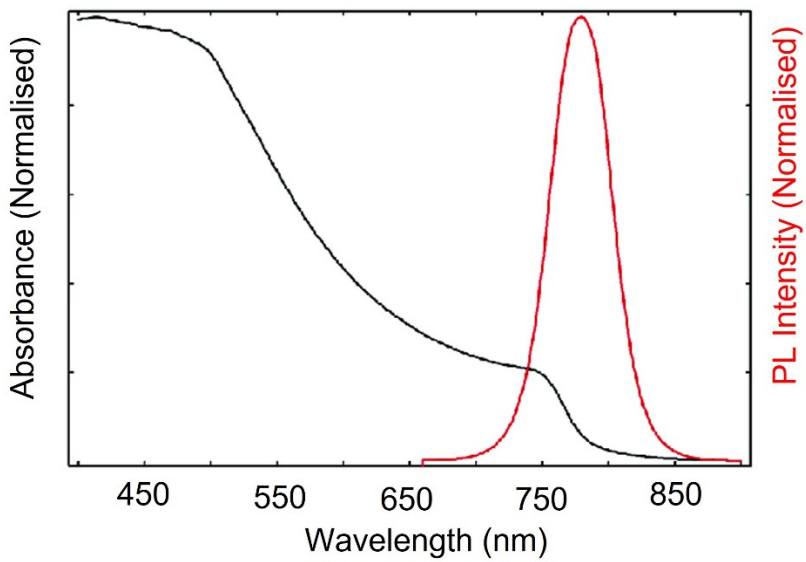

Figure 3. Absorption (black) and photoluminescence emission (red) spectra of a methylammonium lead iodide (MAPI) perovskite.

PL emission is purely a product of the bimolecular recombination of electrons and holes in the conduction and valence band respectively. Nonetheless, analysis of the PL signal can still give valuable information on the non-radiative relaxation processes as well, since the PL emission from a material is directly related to both radiative and nonradiative recombination rates (see the previous section).

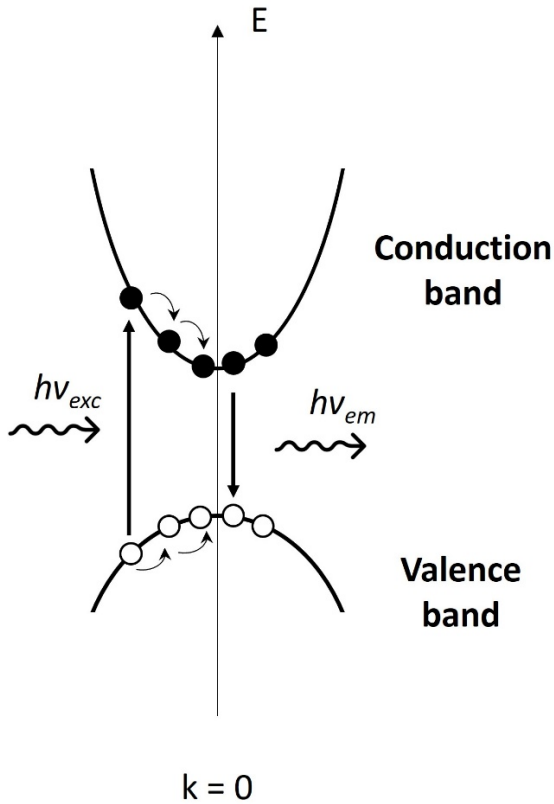

Figure 4. Diagram of the relaxation processes in the momentum-energy space preceding photoluminescence in a direct gap semiconductor.

1.2.4 Photoluminescence Quantum Yield

The ratio of the number of photons emitted to the total number of photons absorbed is referred to as the photoluminescence quantum yield ($PLQY, \Phi$) of the system.

In organic fluorophores, quantum yield is defined as:

$$\Phi = \frac{k_r}{k_r + \sum k_{nr}} \qquad (5)$$

where k_r is the rate constant for radiative relaxation and k_{nr} is the rate constant for all the non-radiative relaxation processes.

We can similarly define the photoluminescence quantum yield of a semiconductor. For each of the SRH and ABC models we get the following two equations respectively:

$$PLQY = \frac{k_r np}{k_r np + k_n n_t p} \qquad (6)$$

$$PLQY = \frac{k_r n^2}{Bn^2 + An} \qquad (7)$$

The PLQY of a semiconductor is a very interesting parameter which can give valuable information regarding the charge recombination processes.

1.3 Photoluminescence Spectroscopy

Photoluminescence spectroscopy is a field of study which employs a number of different techniques that typically involve exciting the sample by a light source (e.g. laser) and detecting the photoluminescence emission. The advantages of these techniques are that they are typically fast and non-destructive while simultaneously providing valuable information on the electronic structure and properties of materials.

1.3.1 Combining Photoluminescence Spectroscopy with Microscopy

A microscope can act as a platform for performing photoluminescence experiments. Fluorescence microscopes are instruments that study characteristics of organic or inorganic substances using fluorescence. The specimen is illuminated by light at a certain wavelength through the objective lens of the microscope, which is absorbed and causes the sample to emit light at longer wavelengths. The emission is collected by the microscope objective and a spectral emission filter is used to separate the excitation light from the fluorescence which is much weaker.

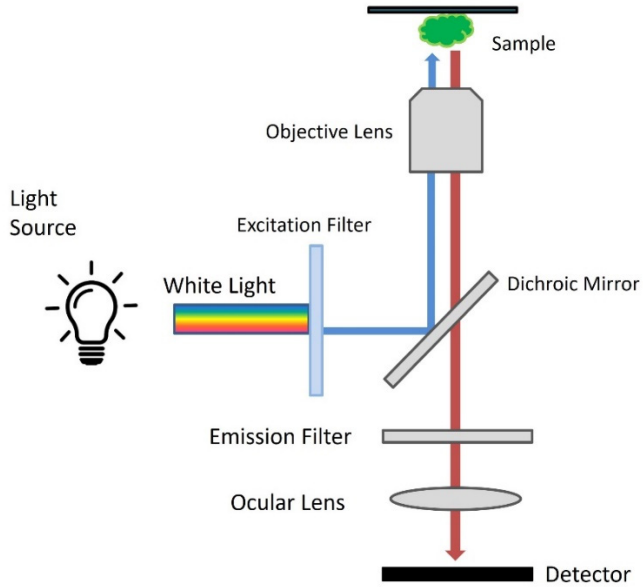

Figure 5. Schematic of a fluorescence microscope.

A light source, excitation filter, dichroic mirror and emission filter are the typical parts of a fluorescence microscope. The spectral excitation and emission properties of the material are considered when selecting the filters and the dichroic mirror.

By combining various spectroscopy techniques with the microscope, we can pinpoint many photophysical and photochemical properties of materials with diffraction-limited spatial resolution.

In the field of MHP semiconductor research, a broad range of PL methodologies have been applied combined with variation of temperature[18–20], and/or the excitation fluence[21–23], voltage dependence[24] and many other parameters. Today many if not all of these methods have been used with PL microscopes as the optical platforms with imaging capabilities to study devices, films, micro and nanocrystals. It is worth mentioning the role of PL microscopy in discovery and study of the fascinating phenomenon of PL blinking of these materials[18,25]. PL microscope combined with various spectroscopy techniques is the main instrument used in this thesis.

1.3.2 Time-Resolved Photoluminescence

Time-resolved photoluminescence (TRPL) is measured by marking the time between the sample excitation by a laser pulse and the arrival of the emitted photon at the detector. TRPL requires a defined “start”, provided by the electronics steering

the laser pulse, and a defined "stop" signal, realized by detection with single-photon sensitive detectors. The measurement of this time delay is repeated many times to account for the statistical nature of the PL emission. The detected events are then sorted into a histogram according to their arrival time which allows reconstruction of the photoluminescence decay. TRPL (Figure 6) is a very powerful tool for the study of fast electronic deactivation processes.

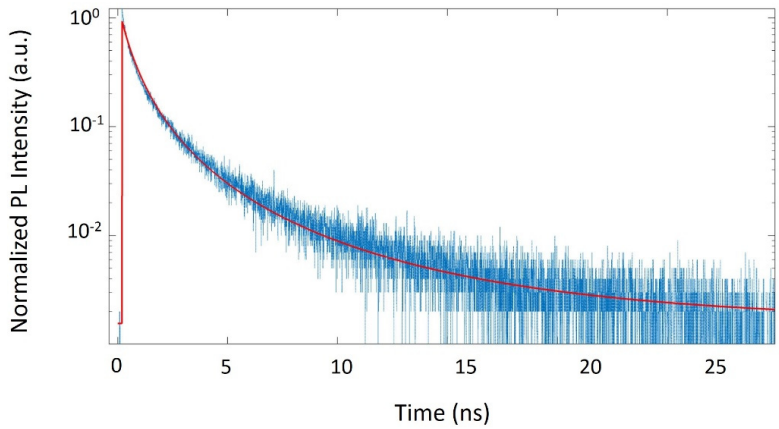

Figure 6. Example of a PL decay histogram. Blue represents the experimental data and the red curve shows a fit of the data.

1.4 Metastable Photoluminescence Processes

1.4.1 Photosensitivity and Degradation

For many luminescent materials, PL intensities are rather stable under constant low power excitation. However, this is not the case for most MHP materials. MHPs are well known for instability and metastability under illumination[25–29]. This is revealed as:

1. Fast induced processes, such as photoluminescence intensity enhancement and bleaching occurring within a time range of milliseconds to minutes of light exposure. Many of these effects can typically be reversed by switching off the excitation light (self-healing).[28,30–32]
2. Permanent changes in the chemical composition and crystal structure of the material when exposed to a combination of light, moisture and

oxygen[33–37]. These processes are generally slower, occurring over several hours or days.

1.4.2 Observer Effect

The observer effect is the phenomenon in which the act of observing a system influences the system being observed[38,39]. One of the most prominent examples is in quantum mechanics and the double slit experiment, which demonstrates the wave-particle duality of matter.[40,41] In this experiment, electron particles are sent through a barrier with two slits. The particles then hit a screen behind the barrier. The pattern that is created on the screen will depend on whether an observer is measuring which slit the particles are going through.

However, the observer effect can also be found in classical physics, as well as psychology and sociology. When measuring voltage for example, the connected voltmeter will draw some current from the circuit, thereby changing the voltage that is being measured.

It is important to consider the observer effect when studying MHPs by spectroscopic methods, since illumination by light will have a significant impact on the properties of the material due to its photosensitive nature, making it difficult to interpret the results of experiments.

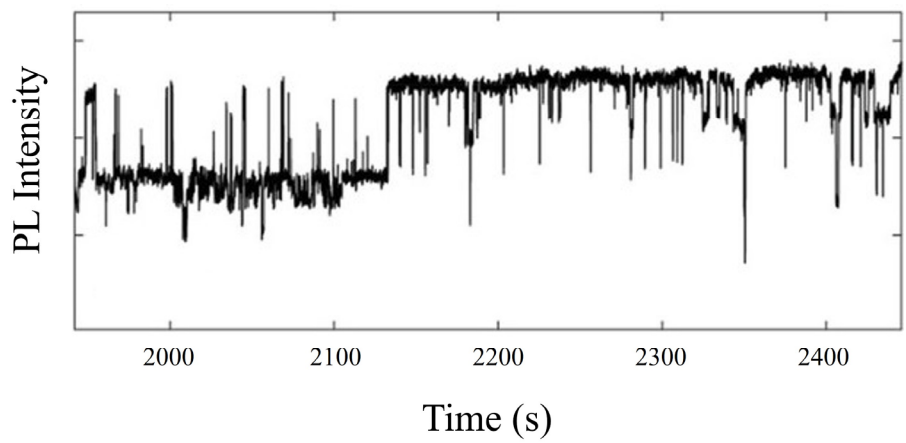

Figure 7. Experimental PL trace of MHP's crystals exhibiting PL blinking. Adapted from [25]

1.4.3 Photoluminescence Blinking

Photoluminescence intermittency, or blinking, is a phenomenon in which a fluorophore, such as a dye, molecule, or quantum dot, exhibits a sudden and random change in its fluorescence intensity under continuous excitation.[42–44] This change can occur on timescales ranging from microseconds to hours and can be observed as an apparent "blinking" of a fluorophore's fluorescence, as shown in Figure 7. Fluorescence intermittency is often used as a tool in single-molecule imaging and spectroscopy.[45–47] Although this phenomenon has been recognized to be characteristic of nanoscale objects, MHP micrometer-sized crystals have exhibited similar effect.[48–51] While the nature of these fluctuations in MHP materials is still under debate, it has been suggested that they are caused by the activation/passivation of extremely efficient quenching-defect states ("supertraps")[29,52]. Several studies have shown these PL fluctuations to be dependent on the size, composition and structure of the sample, as well as the external environment, such as temperature and light intensity[18,25].

Chapter 2 Experimental Methods

2.1 PLQY Portraits

In this chapter we will present a novel experimental photoluminescence measurement technique that involves mapping of the external PLQY in two-dimensional space as a function of both the excitation pulse fluence (P, in photons/cm^2) and excitation pulse frequency (f, in Hz). The acquired PLQY (y axis, log scale) is plotted against the average excitation density (= pulse fluence × repetition rate, W / cm^2, log scale) which we will further on refer to as PLQY or Horse portraits (Figure 8).

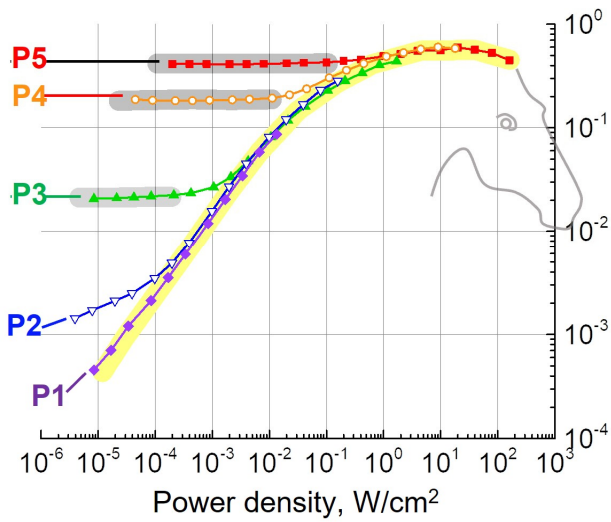

Figure 8. Example of a PLQY - Horse portrait. Each colored line (P1-P5) is a pulse fluence which is scanned over a large range of repetition rates of the pulsed laser (typically from 10KHz to 80MHz). Consecutive pulse fluences (P1-P2 , P2-P3, P3-P4, P4-P5) are different by a factor of 10. Adapted from Paper III.

The name Horse portrait was given to the plot because of the resemblance of the shape to that of a horse neck and mane from the data obtained originally from measurements on methylammonium lead iodide ($MAPbI_3$) MHP materials.

2.1.1 Photoluminescence Intensity Dependence the on Excitation Power Fluence

The more common and simple measurements of photoluminescence intensity dependence on the excitation power – PL(W), involves varying only the excitation fluence for either a continuous-wave (CW) excitation source or a pulsed laser at a specific repetition rate. This is typically achieved by placing a set of neutral attenuation filters (excitation filters) in the path of the laser beam. Several studies on MHPs have employed the PL(W) measurements, often in combination with PL decay, to fit recombination models with the experimental data.[21,23,53,54] Most of these models are based on SRH or ABC recombination theories, sometimes with the addition of diffusion terms. This allows for the extraction of fundamental material parameters, such as recombination rates and trap densities. We will further show, however, that measuring the PL as a function of solely the pulse fluence is not sufficient to obtain unambiguous results.

2.1.2 PL Dependence on the Laser Repetition Rate

When the excitation source is pulsed, we can distinguish two different regimes based on the effect of increasing or decreasing the repetition rate of the laser and monitoring the response of the PLQY.

i) **Single pulse regime**. Here, time (1/f) between consecutive laser pulses is long enough that all excited species created by one pulse (electrons, holes, trapped electron, trapped holes, excitons and so on) have returned to their ground state before the next incoming pulse (Figure 9a). In this case, each excitation has no memory from previous excitation events. In the single pulse regime, the external PLQY remains constant over scanning of the pulse repetition rate, since the PL intensity proportionally scales with the number of pulses within the same time window.

ii) **Quasi-CW regime**. In this condition the system does not have enough time to return to the ground state during the time between two consecutive pulses (Figure 9b). In other words, the population generated by one pulse is dependent on the history of the excitations by the previous pulses. This regime is evident for longer PL decay times (Figure 9b-i) but can also appear in samples with short PL decays where there are still long-lived states present in the system (trapped electrons – free holes or trapped holes – free electrons) (Figure 9b-ii). In the quasi-CW regime, the PL intensity

has a more complex dependence on the scanning of the repetition rate and the PLQY is no longer constant under such scanning.

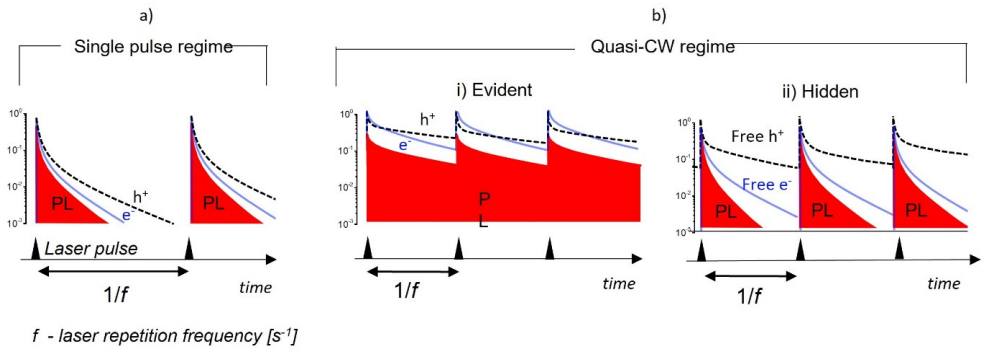

Figure 9. Illustration of the single pulse and quasi-cw regimes. Adapted from Paper III.

2.1.3 PLQY Portraits – Horse Method.

Measuring PLQY as function of average power density with lasers of only a few different repetition rates (Figure 10a) can produce ambiguous results since it is not possible to determine the excitation regime (see previous section). We therefore developed a new methodology of sweeping the pulse frequency over a large range at several fixed pulse fluences and measuring the PLQY (Figure 10b) which provides simple and certain separation between the single pulse and quasi-CW excitation regimes.

One of the challenges that arises is the multiplicity of data points, since we are scanning the excitation power density over pairs of laser pulse fluence and repetition rate. A typical PLQY portrait, like the one shown in Figure 10b, contains approximately 100 measurement points (combinations of pulse fluence (P) and repetition rate (f) pairs).

The average excitation power density (proportional to P*f) ranges over seven orders of magnitude, while the PL intensity is acquired from images obtained from a detector (CCD camera of the PL microscope in our case). To accomplish this in practice, the acquisition time of the detector needs to be substantially increased (up to 5-15mins per image) to compensate for the extremely weak PL signal at the lowest excitation powers. On the other hand, for the high pulse fluences and repetition rates, an additional set of neutral attenuation filters is introduced in the optical path between the sample and the detector (emission filters). It is also crucial to obtain the precise attenuation coefficient of the emission filters to convert the experimentally obtained PL signal to its non-attenuated value. All these parameters

are set and controlled during the experiment through a fully automated system, which will be further discussed in the next chapter.

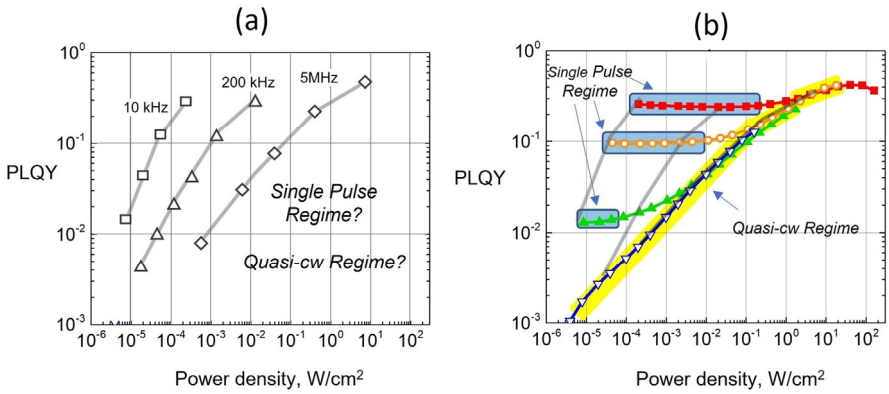

Figure 10. (a) PLQY as a function of power for three different repetition rates, (b) PLQY portrait where the repetition rate of the laser is instead scanned over a braod range for four different pulse fluences (red, orange, green and blue). Yellow shows the quasi-CW regime which is common for all pulse fluences.

The PLQY portraits are complemented with measuring the PL decays at a few combinations of pulse fluences and repetition rates, and together provides a clear and unambiguous criterion to test kinetic models.

2.1.4 PLQY Portrait - Experimental Setup.

The PLQY(f,P) map and PL decays were measured in a custom-built photoluminescence microscopy setup. A pulsed 485 nm laser (Pico Quant, 150 ps pulse width) was used to excite the sample through an objective lens (Olympus 40X, NA = 0.6) of a wide-field fluorescence microscope based on Olympus IX-71. The emission of the sample was then collected by the same objective and captured by one of two detectors. The first detector is an electron multiplying charge-coupled device (EM-CCD) (Princeton Inst. ProEM 512B) for measuring PL(f,P)) .

The second detector is a hybrid photomultiplier/single-photon detector (SPD, Picoquant PMA Hybrid-42) which is connected to a time correlated single photon counting module (Picoquant, Picoharp 300) for the measurement of PL decays kinetics. The instrumental response function width is 200 ps.

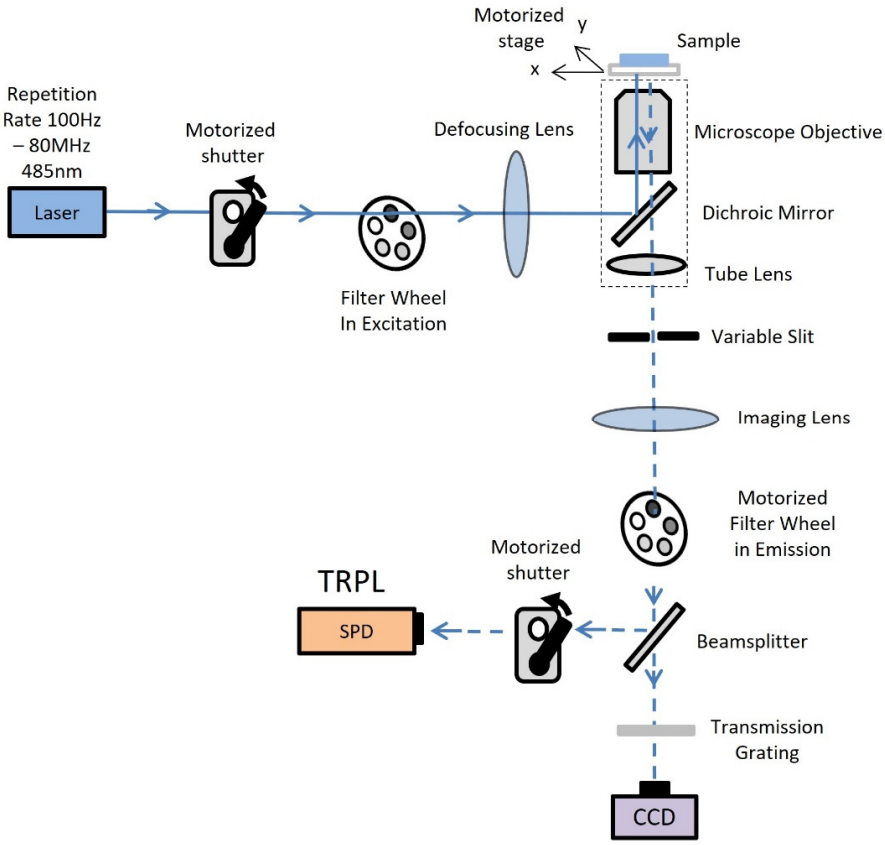

Figure 11. Schematic of the PL microscopy setup designed for measurements of PLQY(f,P) portraits and PL decays.

2.2 PLE Microscopy

Photoluminescence excitation (PLE) is a type of spectroscopic measurement where the wavelength of the excitation light is varied, and the PL intensity is monitored at a fixed emission wavelength of the material being studied.

Through the use of a microscope as the platform for PLE measurements, an advantageous technique is available to measure excitation spectra in situ, while also identifying spatially localized characteristics of the optical and electronic properties of the sample.

2.1.1 PLE – Experimental Setup.

The PLE experiments are conducted using a custom-made microscopy setup (Figure 12). The setup consists of a supercontinuum light source (SuperK Extreme, NKT Photonics) which generates pulsed white laser light. The output beam of the laser is directed to a rotating diffraction grating for creating a narrow (<1 nm) tunable excitation beam from 450 to 800 nm wavelength.

The samples are illuminated using an Olympus 40× objective lens, with a numerical aperture (NA) of 0.6, and the emitted PL is detected by the EM-CCD camera. As a result of this configuration, a wide-field PL image with diffraction-limited resolution is achieved for each of the selected excitation wavelengths. Linear variable long-pass and short-pass filters (3G LVLWP/LVSWP, Delta Optical Thin Film) are employed to significantly suppress (OD > 5) the excitation light before detection, thereby enabling single nanocrystal sensitivity. By illuminating the sample across a range of excitation wavelengths from 450 to 700nm, a set of PL images are obtained that provided all the necessary data for constructing spatially resolved excitation spectra of different parts of the sample.

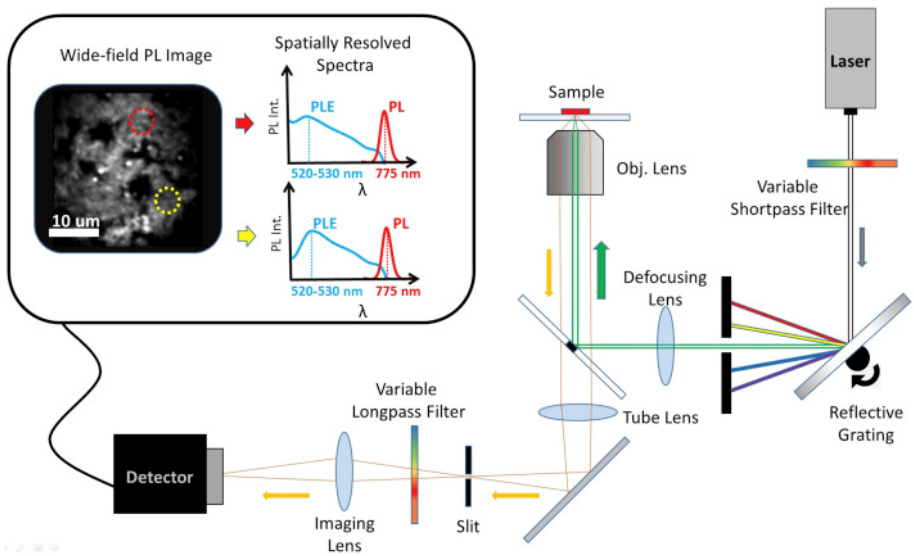

Figure 12. Schematic of photoluminescence excitation microscopy setup. Inserts illustrate $MAPbI_3$ photoluminescence excitation and emission spectra. Adapted from Paper I.

Chapter 3 Robot Microscope

Perovskite material is characterized by their high degree is instability and metastability. The same physical sample can produce significantly different experimental results depending on the measurement conditions. This experimental discrepancy can be attributed to:

- Sample aging. Due to the delicate stability of the material, the same sample, when repeatedly measured over the course of several days or weeks, behaves differently and leading to poor reproducibility of experimental results. Storing the sample in nitrogen and dark environment reduces but still does not prevent changes in the sample.

- Observer effect. Perovskites are especially unstable under light illumination. This means that during any spectroscopy measurements, the act of measuring is affecting the properties of the material and the results of the actual measurement. We have studied this effect to a great extent and introduced various methods to both monitor and mitigate it when we perform our PLQY(f, P) scanning.

Obtaining high degree of reproducibility during the synthesis of MHP samples is also a challenge. Samples prepared by individual scientists using the same preparation recipe very often exhibit different experimental behaviours. Sometimes even two samples prepared by same person and in the same sample-batch shows variations in optoelectronic properties[55].

In order to adequately study and understand the dynamic properties of our material due to i) sample aging and degradation, ii) photo-induced reversible and irreversible processes during the act of measuring (observer effect) as well as iii) sample to sample variation due to difficulties in the synthesis reproducibility, we need to explore a large volume-space of experimental data. We illustrate this by using the PLQY maps as an example (Figure 13). One PLQY(f,P) measurement alone is already a complicated, multi-parameter experiment, and therefore in order for us to practically be able to obtain a large number of PLQY maps it was crucial to build a fully automated experimental system, which we refer to as “Robot microscope”. This was achieved by designing and constructing several custom-built components

in the experimental setup, combining both our own hardware and software and integrating all the devices in one custom-built LabVIEW program, named “SMS-View”, where SMS stands for Single Molecule Spectroscopy group.

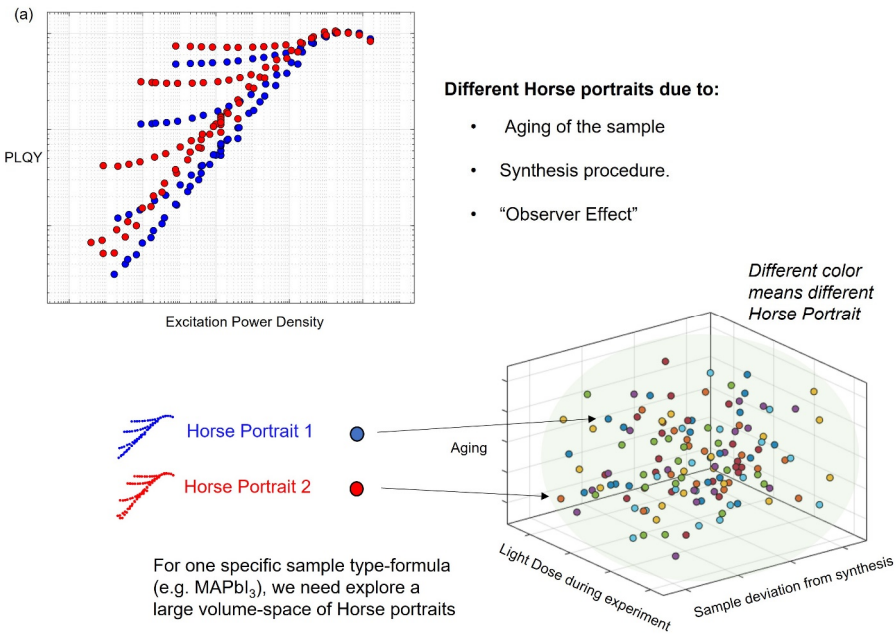

Figure 13. (a) Example of measured PLQY maps (Horse portrains) for two samples of the same formula ($MAPbI_3$). (b) Illustration of the large volume-space of possible experimental outcomes from the different samples of the same MHP material.

The advantage of automating the whole measurement process of Horse portraits is first an immense increase in efficiency. To manually measure a Horse portrait, a person would need to sit in the lab, change parameters, measure and save data for over 100 different measurement points, over a time duration of at least 8-10 hours. The robot microscope can perform the same measurement in less than 2 hours, with no need for supervision from an operator. Furthermore, a fully automated experimental procedure provides greatly improved accuracy of the measurements, eliminates the chance of human error and moreover can perfectly replicate precisely the same experimental conditions for each measurement.

3.1 LabVIEW – Arduino

LabVIEW is a graphical programming language commonly used in laboratory setups to easily control instruments, acquire and analyze data, and create custom user interfaces.

One of the key parts of the robot microscope is a custom-built LabVIEW program that was written and improved upon during the course of this doctoral thesis work. All the instruments and optical elements of the experimental setup are integrated in this "SMS-View" software. Below is a list of the main components which are part of the automated experimental setup.

- **EM-CCD Camera** - main detector for acquiring PL images.
- **Single-photon detector** - to obtain PL decays.
- **Pulsed Laser Module** - changing the repetition rate of the laser pulses.
- **Optical shutters** - Both for eye safety and protection of detectors but also to control and minimize the exposure of the sample to light.
- **Optical filter wheel** – in the excitation path, to change the laser pulse fluence.
- **Optical filter wheels** – in the emission path, in front of each detector to prevent them from saturation.
- **Beamspliter -** to redirect the light between either EM-CCD or the single-photon detector.
- **Motorized Sample Stage –** for high precision positioning of the sample.

For many of these components I designed custom-built systems to move or rotate them with the use of stepper-motors, dc-motors or servos connected to Arduino microcontrollers. An Arduino microcontroller is a cheap and easily programmable circuit board that can act as a communication bridge between the computer and SMS-View software with the physical components of the experimental setup. The SMS-View software sends the necessary instructions to the microcontrollers on how to translate or rotate the components during the automated experiments.

3.2 Horse Table – Recipe

To measure a full Horse portrait, the EM-CCD acquires a series of PL images, one for each combination of the laser repetition rate f and the pulse fluence P. In practice, the "SMS-View" software reads the instructions from input tables. These tables serve as an experiment recipe, and we can easily save and load different recipes

from text files. These recipes contain a step-by-step guide for the robot microscope on how to perform a desired complex experiment.

Experimental Parameters

	Laser Repetiton Rate (Hz)	CCD Exposure time (ms)	Excitation. Filter OD	Emission. Filter OD	Move X-Y Stage (µm)	.....	.....
Step 1.	10.000	6.000	4	1	0	.....	.....
Step 2.	500.000	4000	4	2	20	.....	.....
Step 3.	1.000.000	1000	3	2	0	.....	.....
...	3.000.000	200	3	3	-30	.....	.....
Step 500.	8.000.000	100	2	3	0	.....	.....

Figure 14. Example of an experimental recipe-table that is given as the input to the robot microscope.

Each row of the table is such a step and contains a combination of experimental parameters. The main parameters set in the table include repetition rate of the laser (f), optical filter in the laser beam to regulate the pulse power fluence (Exc.OD), optical attenuation of the emission to protect the detector from saturation (Em.OD) and exposure time of the CCD. The pulse power fluence and the emission attenuation are controlled by two motorized filter wheels placed in the excitation and emission path, respectively, each containing a set of neutral optical density (OD) filters.

3.2 Reference Points

Due to the observer effect and the dynamic changes of the sample during the experiment, we established a procedure involving measuring something that we call a reference point.

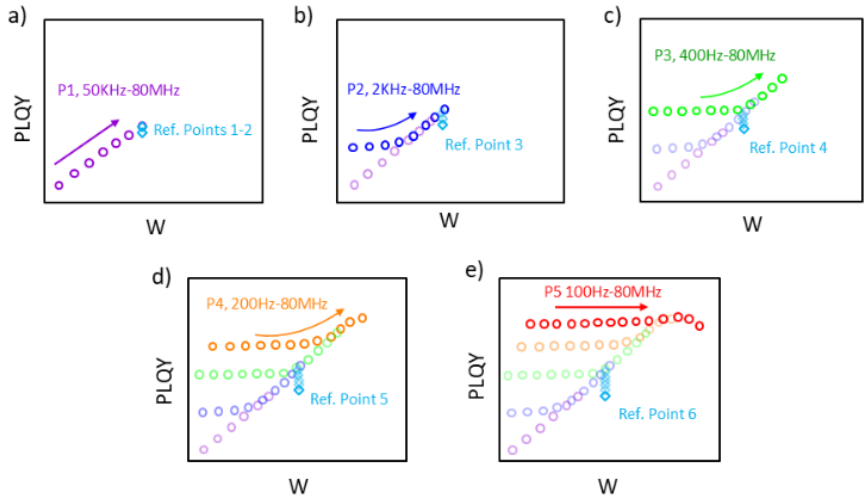

Figure 15. Example sequence in which one complete PL(f,P) map is measured. The entire scan is performed in a sequence of 5 measurements as schematically shown: a) P=P1, f scanned, with the reference points 1 and 2 measured before and after the scan respectively; b) P=P2, f scanned followed by the reference point 3; c) P=P3, f scanned followed by the reference point 4; d) P=P4, f scanned followed by the reference point 5; e) P=P5, f scanned and the full round is finished by measuring the final reference point 6. The change in the reference points in the figure is exaggerated to make it clearly distinguishable.

The reference point is a PL image (from which the PL intensity is determined) acquired at a specific combination of pulse fluence and repetition rate of the laser (P_{ref}, f_{ref}) and measured multiple times throughout one full Horse portrait. What this means is that a measurement starts with acquiring an PL image with reference parameters (P_{ref}, f_{ref}). It then acquires one or more measurement points (P_1, f_1), (P_2, f_2) … then again a reference point (P_{ref}, f_{ref}), and continue to alternate between measurements and the reference. Figure 15 illustrates the build-up of a Horse portrait during an experiment with reference points.

3.3 Synchronization of the Optical Shutter

To minimize photo-induced changes to the sample properties during experiments, the SMS-View program also controls an optical shutter which can block the laser excitation during the idle cycle of the setup, namely while different optical components are physically moving and turning in order to set the desired parameters in preparation for the image acquisitions, and only opens the shutter when everything is set for the EM-CCD to acquire an image. This way we can keep the amount of light soaking the sample to a bare minimum in order to reduce the

observer effect. Furthermore, since the opening-closing of the shutter is computer controlled and takes a known time, we can calculate the dose of light experienced by the sample with good precision.

Here it is important to distinguish between the two types of synchronization between the opening-closing of the shutter and the image acquisition by the EM-CCD:

1) Mode A. The sequence begins with the shutter opening, followed by the camera capturing the PL image. Once the image acquisition is complete, the shutter is closed (as illustrated in Figure 16a). In this scenario, as the EM-CCD initiates PL acquisition, the sample has already been exposed to light for a brief duration. Consequently, the resulting PL image records a later phase of the rapid dynamics of the PL. Also, the sample is exposed to light for time which is longer than necessary for the image acquisition.
2) Mode B. Initially, the camera acquisition starts, followed by the shutter opening and closing before the image acquisition is completed (as depicted in Figure 16b). This synchronization allows us to capture the initial onset of the PL dynamic processes. Also, all PL emitted the sample is detected.

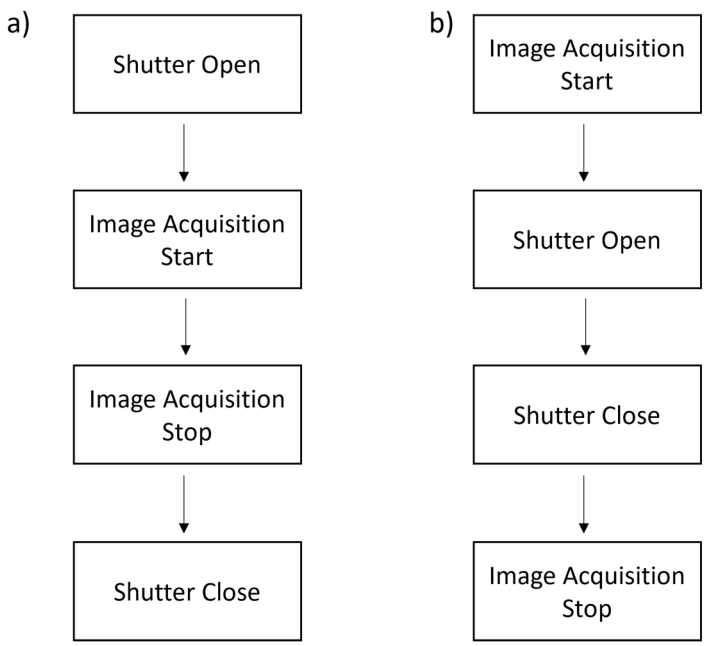

Figure 16. The two synchronization modes of the optical shutter and the CCD camera.

Applying either of these two types of synchronization may have substantial impact on the experimental results in the presence of the observer effect. Such is especially the case if the sample reveals fast dynamic PL properties when it is exposed to light, as illustrated in detail in Figure 17.

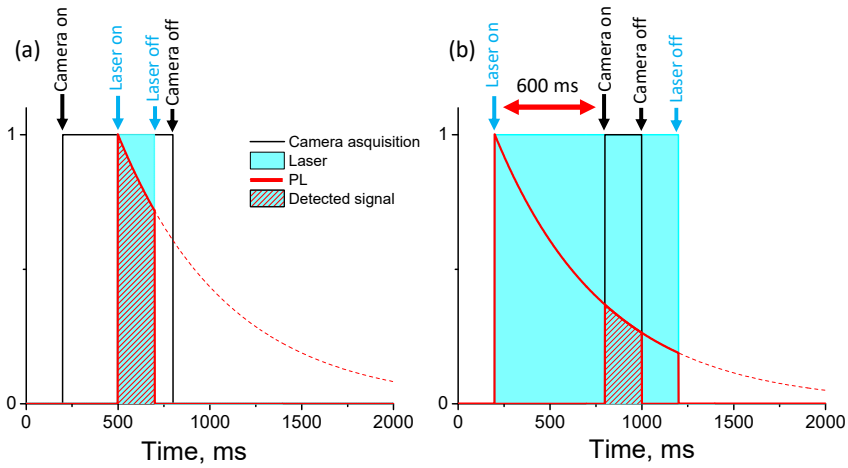

Figure 17. A schematic representation of the critical importance of synchronization between the laser irradiation interval and the signal acquisition window. The evolution of PL intensity after opening the laser shutter is shown by the red line. (a) Data acquisition in mode B, where the effective data acquisition time is equal to the laser irradiation time as both are determined by the laser shutter. (b) Data acquisition in the mode A, where there is a delay between the start of the laser illumination and the start of PL acquisition. This delay is 600 ms in our experiments. The acquisition time is 100 ms in both cases, however, the signal detected in (b) is several times smaller than in (a) due to the PL bleaching over the first 600 ms after opening the laser shutter. Adapted from Paper IV.

Chapter 4 Results & Discussion

4.1 Paper I: Excitation Wavelength Dependence of Photoluminescence Flickering in Degraded $MAPbI_3$ Perovskite and its Connection to Lead Iodide Formation

In Paper 1 we employ the PLE microscopy methodology to in-situ monitor the spatially resolved photo-degradation of methylammonium lead iodide ($MAPbI_3$) thin films. We show that the $MAPbI_3$ samples start exhibiting a distinguishable photoluminescence flickering mainly after degradation and formation of lead iodide (PbI_2). Further we report a clear dependence of the intensity of the PL flickering on the excitation wavelength.

The evolution of the photoluminescence image during the photodegradation of the $MAPbI_3$ film is depicted in Figure 18a–c. The power density in the laser spot caused a faster degradation in the central area, and a much slower degradation at the edges (region 2 in Figure 18c). After 1.5 hours of illumination, the PL in the centre of the excitation spot was largely replaced by PbI_2. Moreover, the regions that still exhibited strong PL (region 3 in Figure. 18c) showed PLE spectrum which has been identified as the result of PbI_2 formation on top of $MAPbI_3$.[56]

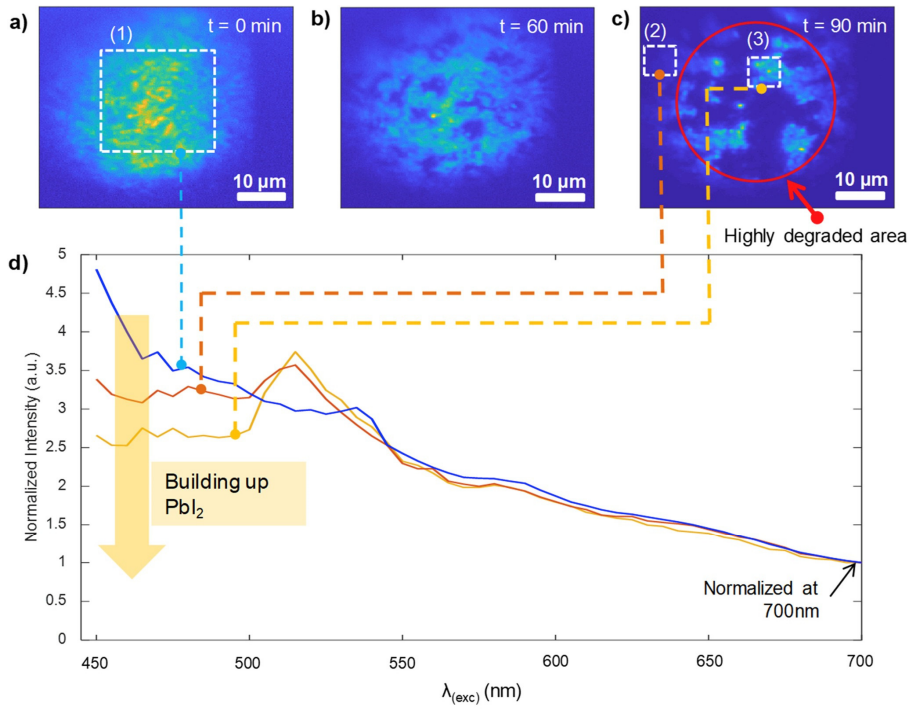

Figure 18. Wide-field photoluminescence images of the same area of a MAPbI3 film after (a) t = 0 (fresh film), (b) t = 60 min and (c) t = 90 min of 1 Sun illumination at ambient conditions. The PL intensity distribution in the fresh film reflects the laser excitation spot profile. (d) Photoluminescence excitation (PLE) spectra at different conditions: blue line - PLE of the fresh film, collected from region (1), orange line – PLE of a slightly degraded region (2), yellow line – PLE of the luminescence coming from region (3) in the highly degraded area. All PLE spectra are normalized at 700 nm. Adapted from Paper I.

For the regions of the sample that had been visibly degraded by photodegradation yet still exhibited luminescence corresponding to $MAPbI_3$ (Fig. 19c, region 3), the PL intensity flickering was much more prominent than in the less degraded parts of the film (Fig. 19c, region 2). This is evidenced by Figure 19b,d. Furthermore, the PL flickering effect fluctuated depending on the excitation wavelength. It was much more significant for $\lambda exc > 530$ nm, as is made clear by comparing the various panels of Figure 18d. In addition, no enhanced flickering occurred under low-energy excitation in region 2, which had only been slightly impacted by the photodegradation (Figure 18b).

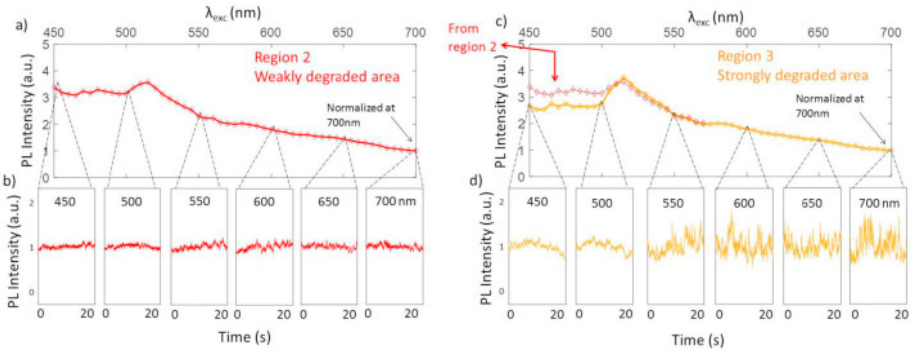

Figure 19. Photoluminescence excitation spectra of regions 2 (panel a)) and 3 (panel c)), see Fig. 2c for the PL image. b), d) - photoluminescence intensity time traces of regions 2 and 3 measured under different excitation wavelengths from 450 to 700 nm with steps of 50 nm. The excitation wavelength is indicated on each graph. Graphs in d) for $\lambda_{exc} \geq 550$ nm show strong PL intensity flickering. Also, see the video in SI for clarity. Adapted from Paper I.

It is possible that the wavelength dependence of the phenomenon may be connected to the excitation wavelength dependence of the photochemical reactions in the material, resulting in the formation or breakdown of the reversible non-radiative centres in $MAPbI_3$. An alternate hypothesis proposes that the PL flickering is diminished due to the restricted mobility of charge carriers, caused by their anchoring in the boundary layer between $MAPbI_3$ and PbI_2.

4.2 Paper II: Impact of Excess Lead Iodide on the Recombination Kinetics in Metal Halide Perovskites

In this work, we analyse the influence of excess lead iodide on the charge carrier recombination kinetics by measuring the PLE spectra and time-resolved photoluminescence as a function of excitation wavelength in the range from 450 to 780 nm. We recognize the presence of PbI_2 in the perovskite film with a distinctive spectroscopic signature in the PLE spectrum. Examining the recombination with and without this feature, we uncover a radiative bimolecular recombination mechanism induced by PbI_2. Investigating the photoluminescence spatially, we determine that this radiative process occurs in a confined region at the PbI_2/perovskite interface, which is only active when charge carriers are generated in PbI_2, thus providing a better understanding of how an excess of PbI_2 may enhance the capabilities of perovskite-based devices.

We carried out parallel PLE studies on 120 consecutive excitation scans, from which we obtained spectra for each scan. The experiments were conducted in ambient air conditions with a relative humidity of 40%, which are ideal for the formation of PbI_2

upon exposure to light[57]. The 2D maps in Figure 20a-b illustrate the changes in absorptance and normalized PLE spectra during the 6-hour measurement, with chosen spectra from three points in time plotted in Figure 20c-d. By examining the absorptance, we can confirm that $MAPbI_3$ decomposes into PbI_2. After 2.5 hours, we observe a noteworthy decrease in the PLE at the particular spectral range between 450 and 520 nm, which we call the "dip". This coincides with the PbI_2 absorption. We propose that this is caused by the filter effect; some of the photons that are absorbed by PbI_2 and generate charge carriers are consequently lost since PbI_2 emission (~520 nm) is blocked in our detection method[58].

In Figure 21, we utilize the time-correlated single-photon counting (TCSPC) approach and fit the PL decays to a stretched exponential function to acquire the average lifetimes. Before any extensive light-soaking, the mean lifetimes from both 450 and 700 nm excitation wavelengths are similar. The monoexponential behavior of the decays implies that the dominant recombination mechanism is trap-assisted. Despite the same photon flux, 450 nm excitation is expected to create a slightly higher carrier generation at the excited surface (where we detect PL), which is reflected in the marginally higher initial amplitude of the decay. Nevertheless, at t = 0 min this disparity in generation is not enough to bring about a dissimilar recombination mechanism.

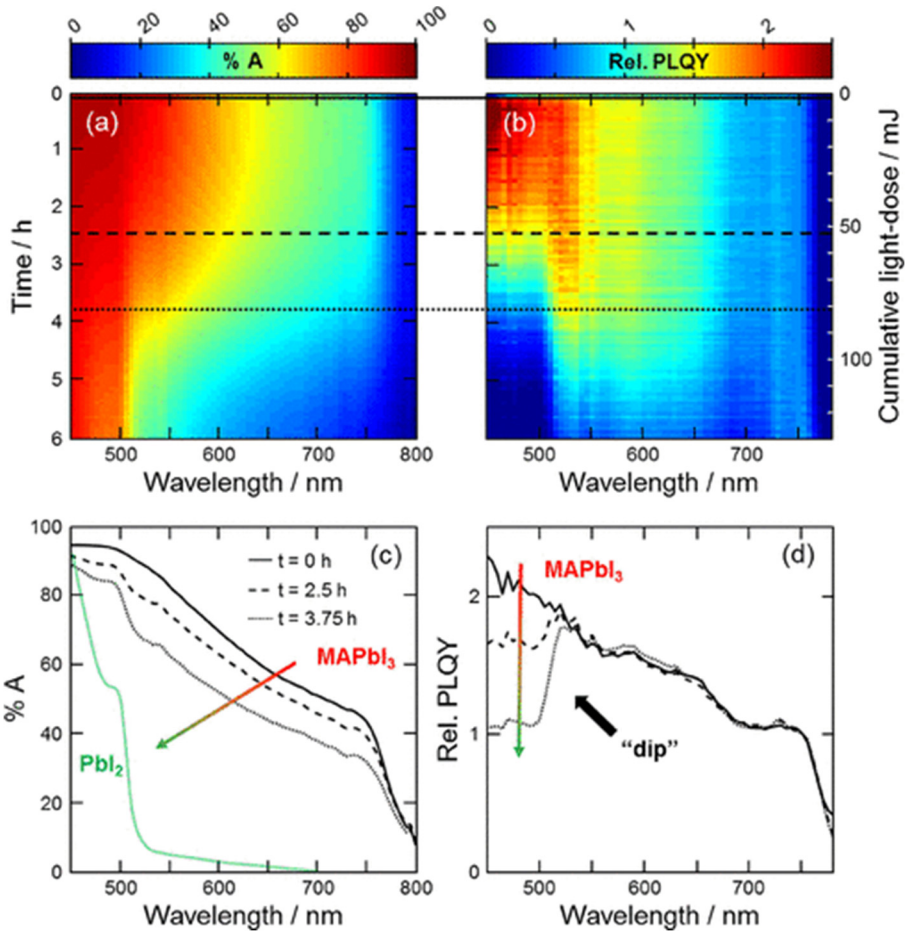

Figure 20. 2D maps showing the temporal evolution of (a) absorptance and (b) normalized PLQY spectra during 6 h of light-soaking. PLQY spectra are normalized at 750 nm. The right vertical axis shows the cumulative light dose throughout the experiment. (c,d) Selected spectra from the two maps at three points in time, t = 0 (solid), 2.5 (dashed), and 3.75 h (dotted). Adapted from Paper II.

In Figure 21b, we can perceive two different traits in the PL kinetics: (i) a boost in the slow decay component, visible directly when light-soaking begins, and (ii) a surge in the fast decay component, which appears after a few hours. Characteristic (i) occurs for both excitation wavelengths, while (ii) is exclusive to 450 nm. We can conclude that (i) was caused by the passivation of nonradiative recombination channels. Moreover, (ii) occurs when there is a marked dip in the PLE spectrum (t = 420 min), which is only observed when exciting in the spectral range of PbI_2 absorption (450–520 nm). As the detection excludes emission from PbI_2, we can infer that the carrier recombination kinetics can be altered in the perovskite simply by the presence of PbI_2, if photons are absorbed by it.

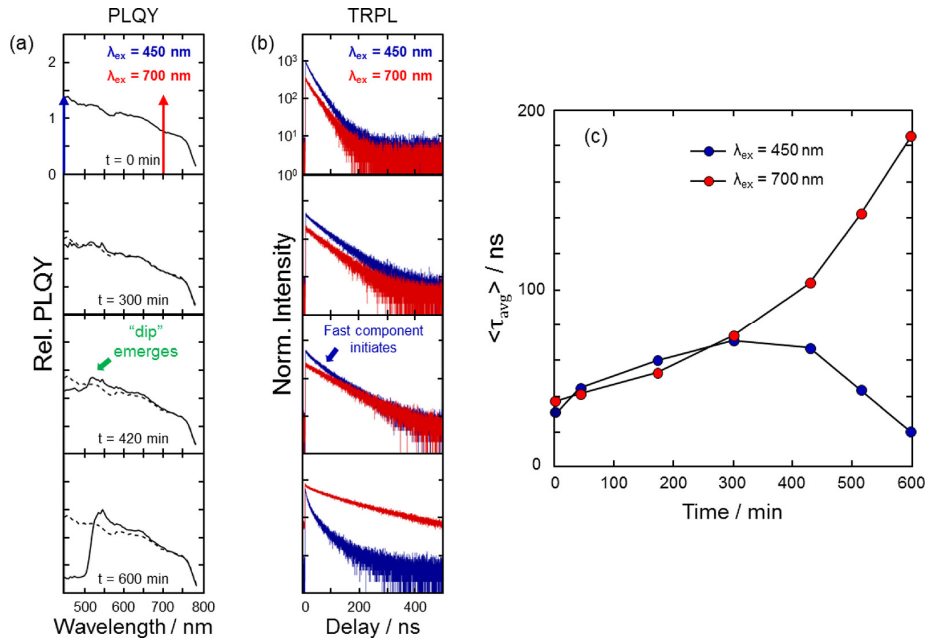

Figure 21. (a) PLE spectra at four instances throughout the 10 h light-soaking experiment. The dashed traces in the bottom three panels represent the PLE at t = 0 min. The vertical scale is the same for all panels. (b) PL decays generated with 450 (blue traces) and 700 nm (red traces) excitation energies at the same time instances as those shown in (a). The vertical scale is the same for all panels. The two excitation wavelengths generating the PL decays in (b) are indicated by blue (450 nm) and red (700 nm) arrows in the top panel of (a). (c) Average lifetimes extracted using stretched exponential fits for both excitation wavelength. Adapted from Paper II.

This study offers a comprehensive insight into the optical characteristics of PbI_2 in $MAPbI_3$ thin films. Employing PLQY and TRPL measurements, we have identified three optical signatures that can be used to determine the presence of PbI_2 in $MAPbI_3$ films: (i) parasitic absorption, (ii) a rapid recombination component in the PL decay, and (iii) a blue shift of PL emission. These features display a dependence on excitation wavelength and the geometry of the sample when PbI_2 is present. Furthermore, these signs are only present when charge carriers are generated in PbI_2 directly. Thus, depending on the configuration of the measurement, one can access information concerning where in the perovskite (sample) PbI_2 is mostly found or begins forming (i.e., at the top or the bottom surface of the film).

4.3 Paper III - Utilizing PLQY Portrait Method on $MAPI_3$ Films to Examine the Validity of the ABC and SRH Models

In this paper, we employ the novel approach for mapping the PLQY described in section 2.1.3 on a set of $MAPI_3$ thin films and try to fit both PLQY portraits and PL decays to validate the ABC and SRH recombination models (Figure 22). Typically, these models are used to semi-quantitatively explain experimental results and derive various rate constants[21,22,53,59–61], often without necessarily taking into account their limitations.

There have been very few attempts to fit both the PL decay and PLQY dependencies of excitation power using ABC/SRH-based models or at least compare the experimental data with theory.[21,23,53,54] However, these methods had limited success due to the frequent existence of huge disparities between experimental data and theoretical fits. Any model of charge carrier dynamics that is believed to be accurate must be able to account for not only typical one-dimensional PLQY(W) data, but also the entire PLQY(f,P) map and PL decays at varied powers and pulse repetition rates.

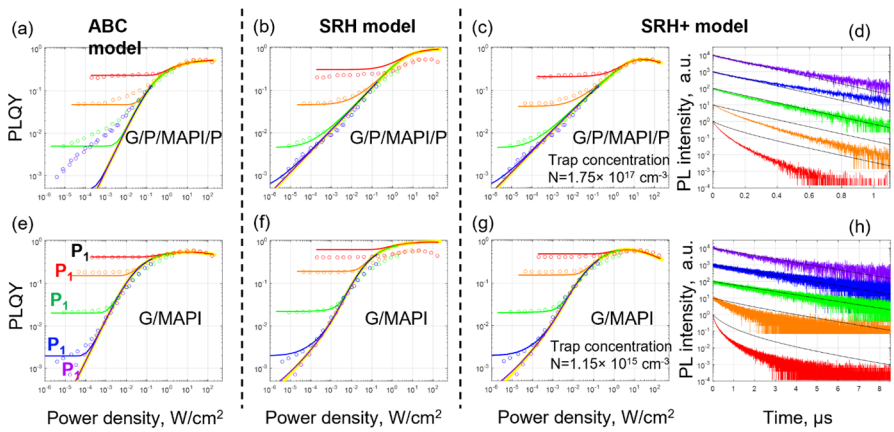

Figure 22. (a) ABC, (b)SRH, (c) SRH+ models applied to the $MAPbI_3$ film and (e) ABC, f (SRH), (g) SRH+ models applied to the $MAPbI_3$ film with PMMA interfaces (G/P/MAPI/P - $MAPbI_3$ deposited on PMMA/glass and then coated by PMMA . In PLQY maps the symbols are experimental points, the lines of the same colour are the theoretical curves. (d) and (h) show experimental and theoretical (black lines) PL decays according to the SRH+ model for both samples, laser repetition rate—100 kHz. The pulse fluences are indicated according to the colour scheme shown in (e) in the whole figure. Adapted from Paper III.

Here, we acquire the PLQY maps on a series of high quality $MAPbI_3$ films with different combination of PMMA interfaces. We emphasize that the (f,P) space (laser

repetition rate, pulse fluence) used in this work is extremely large, with f varying from 100 Hz to 80 MHz (6 orders of magnitude) and P varying over 4 orders of magnitude. We show that neither the ABC nor classical SRH model can fit the acquired PLQY maps across the entire excitation parameter space. To tackle this issue, we develop an enhanced SRH model (SRH+) which accounts for Auger recombination and Auger trapping processes and demonstrates that SRH+ is able to describe and quantitatively fit the PLQY maps over the entire range of excitation conditions with excellent accuracy (Figure 22c,g). PL decays can be also fitted, albeit, with more moderate accuracy (Figure 22d,h).

One possible explanation for the mismatch of the decay rates at high excitation powers might be provided by considering experimental errors. It is well documented that the PL of MHP samples is sensitive to both illumination and environmental conditions, which, may lead to both photodarkening or photobrightening of the sample's PL[27,62–64].

Despite achieving only moderate success at high charge concentrations levels, the outcomes of the SRH+ fitting still represent a substantial improvement over all prior attempts to explain charge carrier dynamics in $MAPbI_3$ samples and allowed us to gain invaluable insights regarding the photophysics of the samples investigated herein and the roles of traps within them.

Upon analysing PLQY maps, it was determined that the concentration of dominant traps within high-quality $MAPbI_3$ approximates $\sim 1.2 \times 10^{15}$ cm^{-3}. Notably, very recent studies using impedance spectroscopy and deep-level transient spectroscopy on $MAPbI_3$ samples prepared using the exact same method yielded nearly identical trap concentration values.[65] This concurrence also aligns remarkably well with the range of values previously proposed by Stranks et al.[21]

An ongoing debate within the perovskite community centres on the impact of defects on charge carrier dynamics in perovskite films. While some studies argue that these defects, often located at grain boundaries, have no significant influence on charge recombination,[66,67] others contend that such defects do affect the optoelectronic quality of the perovskite layer.[68,69] Given these conflicting findings, it becomes evident that traditional PLQY measurements fall short in discerning the role of defects.

We believe that the PLQY(f,P) map represents the most informative signature of a sample concerning its charge recombination pathways and has the potential to help resolve this and other unresolved questions in the field. We anticipate that this non-invasive and straightforward method will have practical applications in the control and optimization of semiconducting materials and the devices built upon them.

4.4 Paper IV - Fast Defect Kinetics in Non-Stoichiometric Hybrid Perovskite ($MAPbI_3$) Films

In this paper we investigate the changes in the photoluminescence response of fractionally non-stoichiometric $MAPbI_3$ perovskite films, whereas previous studies have examined the effect of deviations in precursor stoichiometry on device stability and perovskite response in general.[55,70–73] Using the PLQY mapping approach, samples are tracked over a six-week period. The aging research of the stability of the stoichiometrically altered $MAPbI_3$ films reveals that their PL response varies significantly. In these samples, we found the presence of rapid reversible dynamics that are highly repeatable and evolve over time. We also describe how PL measurements are particularly sensitive to photo-excitation and data gathering techniques, which are typically overlooked in the standard PL studies.

The PLQY maps of $MAPbI_3$ film samples with fractionally deviating stoichiometries (Figure 23c,d) differed markedly from that of standard $MAPbI_3$ films (Figure 23a). They exhibit a reduced absolute PLQY across all excitation regimes. They also display an uncharacteristic initial reduction of PLQY in the single pulse regime as f increases (three grey arrows in Figure 23d). Another untypical characteristic appears as a “discontinuity” within the single regime at the highest pulse fluence, highlighted by the double-sided arrows in Figure 23c,d. These last two features have their origin traced back to the observer effect, related to the photosensitivity of the material and the precise details of the sample light exposure controlled by a shutter as previously explained in section 3.3.

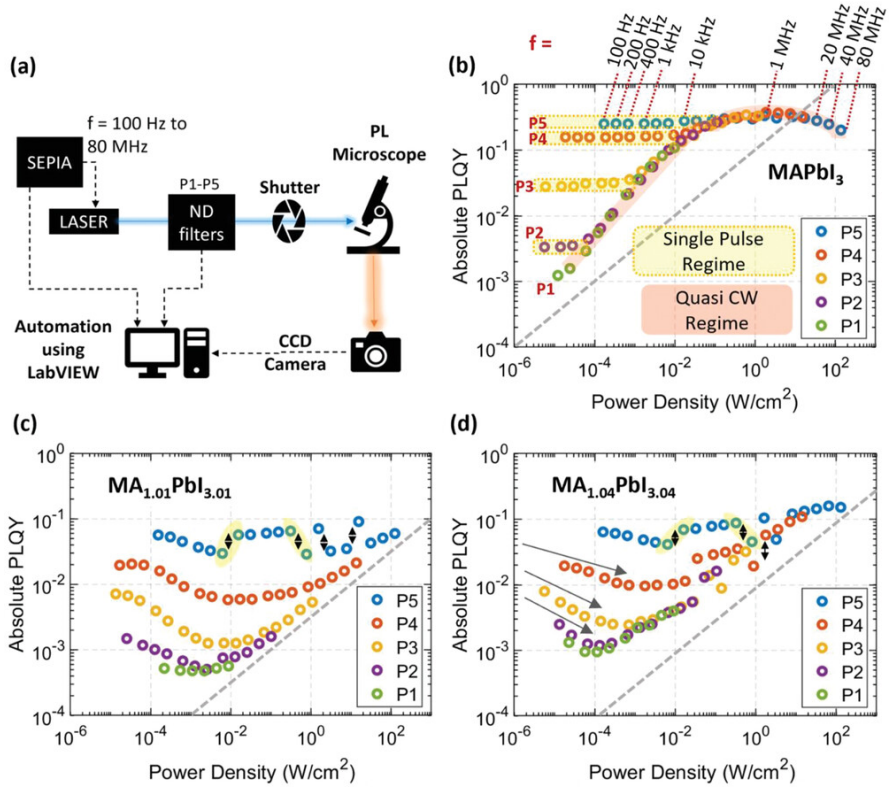

Figure 23. A schematic representation of the setup for acquisition of PLQY(f,P) maps. PLQY maps of b) $MAPbI_3$, c) $MA_{1.04}PbI_{3.04}$, and d) $MA_{1.1}PbI_{3.1}$ films. The map is formed by plotting together a family of 5 curves of PLQY versus Power Density. Each curve is obtained for its own pulse fluence, P_n. P1 is the lowest and P5 is the highest pulse fluence (in photons/cm^2/pulse). The scanning of the laser repetition rate f is illustrated in (b) for pulse fluence P5. See the text for details. The grey dash lines show the square root dependence between the excitation power density and PLQY, which aids to compare the slopes of the quasi-CW-regime of the samples. Different excitation regimes are marked in (b). Adapted from Paper IV.

After identifying the causes of the artifacts in the PLQY maps, we investigate how these maps evolve as the samples undergo storage. It is worth noting that we consistently employed exactly the same data acquisition procedure, enabling direct comparisons between maps of different samples and those of the same samples measured at varying storage durations. Our findings indicate that the artifacts stemming from defect dynamics in over-stoichiometric samples diminish as the films age (Figure 24).

As evidenced by the PLQY maps, PLQY increases with the aging of the samples, and the abrupt jumps caused by fast dynamics at high excitation power also decrease. While the PLQY map for the sample aged six weeks still exhibits artifacts, such as non-constant PLQY in the single-pulse regime, it has significantly converged with the reference stoichiometric MAPI (as compared to Figure 23b).

This substantial shift in PL response signifies a healing process occurring within the sample. We propose that the excessive iodide within the crystal structure (inherent to over-stoichiometric samples), initially migrates to the surface of the grains and subsequently departs from the surface over time, particularly upon exposure to oxygen and light illumination. This process aligns with the discussion presented by Goetz et al[74], where the healing of an over-stoichiometric MAPI film was observed following deliberate photo-oxidation.

The evolution of the PLQY maps for the considerably over-stoichiometric $MA_{1.1}PbI_{3.1}$ is illustrated in the lower row of Figure 24. While the PLQY values exhibit a slight increase with the sample's aging, the anomalies stemming from rapid light-induced defect dynamics persist at the same level. This indicates that when the extent of over-stoichiometry surpasses a certain threshold, the sample does not naturally revert to its standard state over time. Even after an extended period of storage, it maintains charge carrier and defect dynamics significantly distinct from those of the stoichiometric MAPI film.

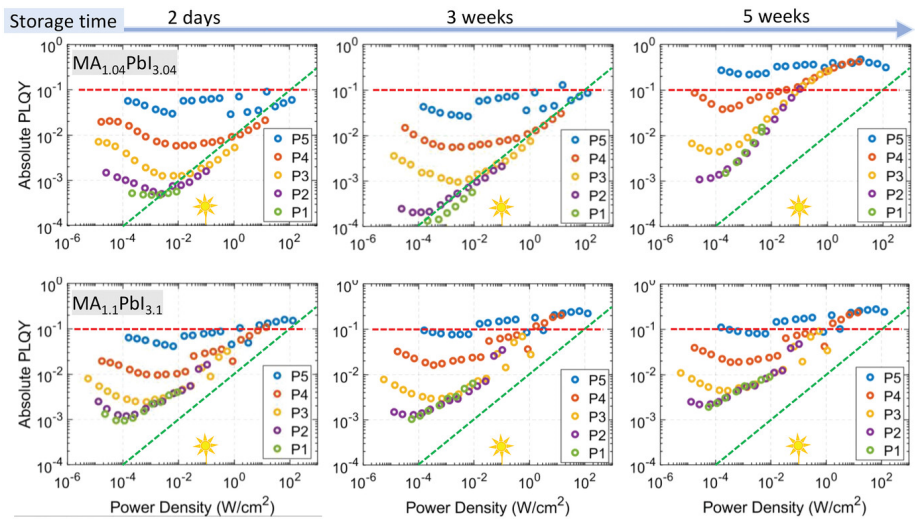

Figure 24. A series of PLQY(f,P) maps demonstrating the evolution of the response of the non-stoichiometric MAPI films as a function of the storage time after synthesis. Top raw—the slightly over-stoichiometric $MA_{1.04}PbI_{3.04}$, bottom raw—the significantly over-stoichiometric $MA_{1.1}PbI_{3.1}$ films. Red horizontal dash line shows PLQY = 10%, the tilted green dash line is the square root dependence (slope 0.5 in log-log scale) expected for the quasi-CW regime for the case of photodoping without trap saturation. These lines aid comparison of the plots between each other. The "sun" marks the excitation power density of 0.1 W cm^{-2}. Adapted from Paper IV.

There still remains a lack of comprehensive understanding regarding the specific defects responsible for the apparent photosensitivity observed in MAPI by researchers. Previous studies suggests that iodide interstitials, which naturally occur

at significant levels in over-stoichiometric samples, are, to some extent, a contributing factor[26,27,75,76]. In these over-stoichiometric samples, there is also an excess of MA^+ counter ions. However, it is generally understood that these excess MA^+ ions play a far less significant role in non-radiative recombination processes.[65]

Due to the automated experimental process and the distinctive mapping across extensive parameter space encompassing f and P, we can promptly recognize certain samples displaying atypical characteristics. These samples should be approached cautiously for analysis, particularly in the light of their photosensitivity. In a strict sense, for materials featuring photosensitive defect concentrations, conventional spectroscopic techniques and established theoretical models may not be entirely suitable or reliable for comprehensive analysis.

Chapter 5 Conclusions

The findings presented in Paper I highlight the successful utilization of PLE microscopy for real-time monitoring of spatially resolved photodegradation in $MAPbI_3$ thin films. Notably, the emergence of discernible photoluminescence flickering withing the samples is prominently associated with the degradation process and the subsequent formation of PbI_2. Additionally, our study reveals a significant correlation between the intensity of observed PL flickering and the excitation wavelength used.

In Paper II we utilize PLQY and TRPL measurements to successfully identify three distinct optical markers that serve to indicate the presence of PbI_2 within $MAPbI_3$ films. These characteristics exhibit variations based on the excitation wavelength and sample geometry, specifically in cases where PbI_2 is detected. Consequently, depending on the measurement configuration, researchers can access valuable insights into the specific location of PbI_2 within the perovskite film-providing insights into whether it is primarily concentrated at the film's top or bottom surface, or where its formation initiates.

In Papers III and IV we introduced and applied a novel experimental methodology, incorporating PL measurements within a two-dimensional parameter space of laser pulse excitation fluence and pulse repetition frequency. These maps allow for distinction between single-pulse and quasi-continuous excitation regimes and provide a useful tool for examining the validity of commonly employed and future kinetic models of charge recombination. This approach has further revealed distinct features (fingerprints) withing the PLQY maps that enable clear differentiation between samples and by their electronic properties.

In conclusion, perovskite metal halides hold immense promise as a class of materials with remarkable optoelectronic properties, making them attractive candidates for various technological applications. However, the pursuit of harnessing their potential is not without its challenges. We show the necessity of designing meticulous experiments, implementing advanced measurement techniques, and adopting controlled environments in order to mitigate the observer effect's impact. Moreover, since experimental results on MHP's are strongly influenced on synthesis methods, environmental condition, and measurement protocols, interdisciplinary collaborations and standardized practices become essential to ensure the reproducibility and reliability of results across different research groups.

References

1. Jena, A. K., Kulkarni, A. & Miyasaka, T. Halide Perovskite Photovoltaics: Background, Status, and Future Prospects. *Chem Rev* **119**, 3036–3103 (2019).
2. Schmidt-Mende, L. *et al.* Roadmap on organic–inorganic hybrid perovskite semiconductors and devices. *APL Mater* **9**, 109202 (2021).
3. Dong, H., Zhang, C., Liu, X., Yao, J. & Zhao, Y. S. Materials chemistry and engineering in metal halide perovskite lasers. *Chem Soc Rev* **49**, 951–982 (2020).
4. Xie, C., Liu, C.-K., Loi, H.-L. & Yan, F. Perovskite-Based Phototransistors and Hybrid Photodetectors. *Adv Funct Mater* **30**, 1903907 (2020).
5. Park, N.-G. Perovskite solar cells: an emerging photovoltaic technology. *Materials Today* **18**, 65–72 (2015).
6. Faridi, A. W. *et al.* Synthesis and Characterization of High-Efficiency Halide Perovskite Nanomaterials for Light-Absorbing Applications. *Ind Eng Chem Res* **62**, 4494–4502 (2023).
7. Agbaoye, R. O., Akinlami, J. O., Afolabi, T. A. & Adebayo, G. A. Unraveling the Stable Phase, High Absorption Coefficient, Optical and Mechanical Properties of Hybrid Perovskite CH3NH3PbxMg1–xI3: Density Functional Approach. *J Inorg Organomet Polym Mater* **30**, 299–309 (2020).
8. Tablero Crespo, C. Absorption coefficients data of lead iodine perovskites using 14 different organic cations. *Data Brief* **27**, 104636 (2019).
9. Habibi, M., Zabihi, F., Ahmadian-Yazdi, M.-R. & Eslamian, M. Progress in emerging solution-processed thin film solar cells – Part II :Perovskite solar cells. *RenewableandSustainableEnergyReviews* **62**, 10–12 (2016).
10. Kulkarni, S. A. *et al.* Band-gap tuning of lead halide perovskites using a sequential deposition process. *J Mater Chem A Mater* **2**, 9221–9225 (2014).
11. Ou, Q. *et al.* Band structure engineering in metal halide perovskite nanostructures for optoelectronic applications. *Nano Materials Science* **1**, (2019).

12. Ju, D. *et al.* Tunable Band Gap and Long Carrier Recombination Lifetime of Stable Mixed CH3NH3PbxSn1–xBr3 Single Crystals. *Chemistry of Materials* **30**, 1556–1565 (2018).

13. Kojima, A., Teshima, K., Shirai, Y. & Miyasaka, T. Organometal halide perovskites as visible-light sensitizers for photovoltaic cells. *J Am Chem Soc* **131**, 6050–6051 (2009).

14. Best Research-Cell Efficiency Chart | Photovoltaic Research | NREL. https://www.nrel.gov/pv/cell-efficiency.html.

15. Shockley, W. & Read, W. T. Statistics of the Recombinations of Holes and Electrons. *Physical Review* **87**, 835–842 (1952).

16. Hall, R. N. Electron-Hole Recombination in Germanium. *Physical Review* **87**, 387 (1952).

17. Shen, Y. C. *et al.* Auger recombination in InGaN measured by photoluminescence. *Appl Phys Lett* **91**, 141101 (2007).

18. Gerhard, M. *et al.* Microscopic insight into non-radiative decay in perovskite semiconductors from temperature-dependent luminescence blinking. *Nat Commun* **10**, 1698 (2019).

19. Dobrovolsky, A., Merdasa, A., Unger, E. L., Yartsev, A. & Scheblykin, I. G. Defect-induced local variation of crystal phase transition temperature in metal-halide perovskites. *Nat Commun* **8**, 34 (2017).

20. Wright, A. D. *et al.* Electron–phonon coupling in hybrid lead halide perovskites. *Nat Commun* **7**, 11755 (2016).

21. Stranks, S. D. *et al.* Recombination Kinetics in Organic-Inorganic Perovskites: Excitons, Free Charge, and Subgap States. *Phys Rev Appl* **2**, 34007 (2014).

22. Johnston, M. B. & Herz, L. M. Hybrid Perovskites for Photovoltaics: Charge-Carrier Recombination, Diffusion, and Radiative Efficiencies. *Acc Chem Res* **49**, 146–154 (2016).

23. Manger, L. H. *et al.* Global Analysis of Perovskite Photophysics Reveals Importance of Geminate Pathways. *The Journal of Physical Chemistry C* **121**, 1062–1071 (2017).

24. Stolterfoht, M. *et al.* Voltage-Dependent Photoluminescence and How It Correlates with the Fill Factor and Open-Circuit Voltage in Perovskite Solar Cells. *ACS Energy Lett* **4**, 2887–2892 (2019).

25. Seth, S. *et al.* Presence of Maximal Characteristic Time in Photoluminescence Blinking of MAPbI3 Perovskite. *Adv Energy Mater* **11**, 2102449 (2021).

26. Motti, S. G. *et al.* Controlling competing photochemical reactions stabilizes perovskite solar cells. *Nat Photonics* **13**, 532–539 (2019).

27. Motti, S. G. *et al.* Defect Activity in Lead Halide Perovskites. *Advanced Materials* **31**, 1901183 (2019).

28. Galle, M. H. J. J., Li, J., Frantsuzov, P. A., Basché, T. & Scheblykin, I. G. Self-Healing Ability of Perovskites Observed via Photoluminescence Response on Nanoscale Local Forces and Mechanical Damage. *Advanced Science* **10**, 2204393 (2023).

29. Merdasa, A. *et al.* "Supertrap" at Work: Extremely Efficient Nonradiative Recombination Channels in MAPbI3 Perovskites Revealed by Luminescence Super-Resolution Imaging and Spectroscopy. *ACS Nano* **11**, 5391–5404 (2017).

30. Domanski, K. *et al.* Migration of cations induces reversible performance losses over day/night cycling in perovskite solar cells. *Energy Environ Sci* **10**, 604–613 (2017).

31. Ceratti, D. R. *et al.* Self-Healing and Light-Soaking in MAPbI3: The Effect of H2O. *Advanced Materials* **34**, 2110239 (2022).

32. Cahen, D. & Lubomirsky, I. Self-Repairing Energy Materials: Sine Qua Non for a Sustainable Future. *Acc Chem Res* **50**, 573–576 (2017).

33. Misra, R. K. *et al.* Temperature- and Component-Dependent Degradation of Perovskite Photovoltaic Materials under Concentrated Sunlight. *J Phys Chem Lett* **6**, 326–330 (2015).

34. Yang, J., Siempelkamp, B. D., Liu, D. & Kelly, T. L. Investigation of CH3NH3PbI3 Degradation Rates and Mechanisms in Controlled Humidity Environments Using in Situ Techniques. *ACS Nano* **9**, 1955–1963 (2015).

35. Purev-Ochir, B. *et al.* Oxygen-Induced Reversible Degradation of Perovskite Solar Cells. *Solar RRL* **7**, 2300127 (2023).

36. Senocrate, A. *et al.* Interaction of oxygen with halide perovskites. *J Mater Chem A Mater* **6**, 10847–10855 (2018).

37. Zheng, D. G. & Kim, D. H. Degradation mechanisms of perovskite light-emitting diodes under electrical bias. **12**, 451–476 (2023).

38. Sassoli de Bianchi, M. The Observer Effect. *Found Sci* **18**, 213–243 (2013).

39. Baclawski, K. The Observer Effect. in *2018 IEEE Conference on Cognitive and Computational Aspects of Situation Management (CogSIMA)* 83–89 (2018). doi:10.1109/COGSIMA.2018.8423983.

40. Young, T. II. The Bakerian Lecture. On the theory of light and colours. *Philos Trans R Soc Lond* **92**, 12–48 (1997).

41. Howie, A., Ffowcs Williams, J. E., Howie, A. & Ffowcs Williams, J. E. Preface. *Philosophical Transactions of the Royal Society of London. Series A: Mathematical, Physical and Engineering Sciences* **360**, 805–806 (2002).

42. Shi, J. *et al.* All-optical fluorescence blinking control in quantum dots with ultrafast mid-infrared pulses. *Nat Nanotechnol* **16**, 1355–1361 (2021).

43. Galland, C. *et al.* Two types of luminescence blinking revealed by spectroelectrochemistry of single quantum dots. *Nature* **479**, 203–207 (2011).

44. Frantsuzov, P. A. & Marcus, R. A. Explanation of quantum dot blinking without the long-lived trap hypothesis. *Phys Rev B* **72**, 155321 (2005).

45. Lelek, M. *et al.* Single-molecule localization microscopy. *Nature Reviews Methods Primers* **1**, 39 (2021).

46. Chien, F.-C., Lin, C.-Y. & Abrigo, G. Single-Molecule Blinking Fluorescence Enhancement by Surface Plasmon-Coupled Emission-Based Substrates for Single-Molecule Localization Imaging. *Anal Chem* **93**, 15401–15411 (2021).

47. Püntener, S. & Rivera-Fuentes, P. Single-Molecule Peptide Identification Using Fluorescence Blinking Fingerprints. *J Am Chem Soc* **145**, 1441–1447 (2023).

48. Gerhard, M. *et al.* Heterogeneities and Emissive Defects in MAPbI3 Perovskite Revealed by Spectrally Resolved Luminescence Blinking. *Adv Opt Mater* **9**, 2001380 (2021).

49. Pathoor, N. *et al.* Fluorescence Blinking Beyond Nanoconfinement: Spatially Synchronous Intermittency of Entire Perovskite Microcrystals. *Angewandte Chemie International Edition* **57**, 11603–11607 (2018).

50. Pathoor, N. & Chowdhury, A. Spatially Correlated Blinking of Perovskite Micro-crystals: Deciphering Effective Modes of Communication between Distal Photoexcited Carriers. *ACS Photonics* **10**, (2022).

51. Halder, A., Pathoor, N., Chowdhury, A. & Sarkar, S. Photoluminescence Flickering of Micron Sized Crystals of Methylammonium Lead Bromide:

Effect of Ambience and Light Exposure. *The Journal of Physical Chemistry C* **122**, (2018).

52. Eremchev, I. Yu., Tarasevich, A. O., Li, J., Naumov, A. V & Scheblykin, I. G. Lack of Photon Antibunching Supports Supertrap Model of Photoluminescence Blinking in Perovskite Sub-Micrometer Crystals. *Adv Opt Mater* **9**, 2001596 (2021).

53. Saba, M. *et al.* Correlated electron-hole plasma in organometal perovskites. *Nat Commun* **5**, (2014).

54. Trimpl, M. J. *et al.* Charge-Carrier Trapping and Radiative Recombination in Metal Halide Perovskite Semiconductors. *Adv Funct Mater* **30**, (2020).

55. Goetz, K. P. & Vaynzof, Y. The Challenge of Making the Same Device Twice in Perovskite Photovoltaics. *ACS Energy Lett* **7**, 1750–1757 (2022).

56. Merdasa, A. *et al.* Impact of Excess Lead Iodide on the Recombination Kinetics in Metal Halide Perovskites. *ACS Energy Lett* **4**, 1370-1378 (2019).

57. Yang, J., Siempelkamp, B. D., Liu, D. & Kelly, T. L. Investigation of CH3NH3PbI3 Degradation Rates and Mechanisms in Controlled Humidity Environments Using in Situ Techniques. *ACS Nano* **9**, 1955–1963 (2015).

58. Melvin, A. A. *et al.* Lead iodide as a buffer layer in UV-induced degradation of CH3NH3PbI3 films. *Solar Energy* **159**, 794–799 (2018).

59. Feldmann, S. *et al.* Photodoping through local charge carrier accumulation in alloyed hybrid perovskites for highly efficient luminescence. *Nat Photonics* **14**, 123–128 (2020).

60. DeQuilettes, D. W. *et al.* Tracking Photoexcited Carriers in Hybrid Perovskite Semiconductors: Trap-Dominated Spatial Heterogeneity and Diffusion. *ACS Nano* **11**, 11488–11496 (2017).

61. Kang, G. *et al.* Electron trapping and extraction kinetics on carrier diffusion in metal halide perovskite thin films. *J Mater Chem A Mater* **7**, 25838–25844 (2019).

62. Tian, Y. *et al.* Mechanistic insights into perovskite photoluminescence enhancement: Light curing with oxygen can boost yield thousandfold. *Physical Chemistry Chemical Physics* **17**, 24978–24987 (2015).

63. Andaji-Garmaroudi, Z., Anaya, M., Pearson, A. J. & Stranks, S. D. Photobrightening in Lead Halide Perovskites: Observations, Mechanisms, and Future Potential. *Adv Energy Mater* **10**, (2020).

64. Fassl, P. *et al.* Fractional deviations in precursor stoichiometry dictate the properties, performance and stability of perovskite photovoltaic devices. *Energy Environ Sci* **11**, 3380–3391 (2018).

65. Reichert, S. *et al.* Probing the ionic defect landscape in halide perovskite solar cells. *Nat Commun* **11**, (2020).

66. Yang, M. *et al.* Do grain boundaries dominate non-radiative recombination in CH3NH3PbI3 perovskite thin films? *Physical Chemistry Chemical Physics* **19**, 5043–5050 (2017).

67. Yin, W. J., Shi, T. & Yan, Y. Unique properties of halide perovskites as possible origins of the superior solar cell performance. *Advanced Materials* **26**, 4653–4658 (2014).

68. Xu, W. *et al.* Precisely Controlling the Grain Sizes with an Ammonium Hypophosphite Additive for High-Performance Perovskite Solar Cells. *Adv Funct Mater* **28**, (2018).

69. Ren, X. *et al.* Modulating crystal grain size and optoelectronic properties of perovskite films for solar cells by reaction temperature. *Nanoscale* **8**, 3816–3822 (2016).

70. Taylor, A. D. *et al.* A general approach to high-efficiency perovskite solar cells by any antisolvent. *Nat Commun* **12**, 1878 (2021).

71. Odabaşı, Ç. & Yıldırım, R. Assessment of Reproducibility, Hysteresis, and Stability Relations in Perovskite Solar Cells Using Machine Learning. *Energy Technology* **8**, 1901449 (2020).

72. Jamal, M. S. *et al.* Fabrication techniques and morphological analysis of perovskite absorber layer for high-efficiency perovskite solar cell: A review. *Renewable and Sustainable Energy Reviews* **98**, 469–488 (2018).

73. Chen, Z. *et al.* Processing and Preparation Method for High-Quality Opto-Electronic Perovskite Film. *Front Mater* **8**, (2021).

74. Goetz, K. P. *et al.* Remarkable performance recovery in highly defective perovskite solar cells by photo-oxidation. *J Mater Chem C Mater* **11**, 8007–8017 (2023).

75. DeQuilettes, D. W. *et al.* Photo-induced halide redistribution in organic-inorganic perovskite films. *Nat Commun* **7**, (2016).

76. Fassl, P. *et al.* Effect of density of surface defects on photoluminescence properties in MAPbI3 perovskite films. *J Mater Chem C Mater* **7**, 5285–5292 (2019).

Printed by Media-Tryck, Lund 2023 NORDIC SWAN ECOLABEL 3041 0903

Faculty of Science
Department of Chemistry
Division Chemical Physics

ISBN 978-91-7422-998-1